The locus coeruleus broadcasts prediction errors across the cortex to promote sensorimotor plasticity

Rebecca Jordan[1,3,4] & Georg B. Keller[1,2]

[1]*Friedrich Miescher Institute for Biomedical Research, Basel, Switzerland.*
[2]*Faculty of Sciences, University of Basel, Basel, Switzerland.*
[3]*Current address: Simons Initiative for the Developing Brain, University of Edinburgh, 1 George Square, EH8 9JZ, Edinburgh, United Kingdom.*
[4]*Correspondence to:* rjordan3@ed.ac.uk

ABSTRACT

Prediction errors are differences between expected and actual sensory input and are thought to be key computational signals that drive learning related plasticity. One way that prediction errors could drive learning is by activating neuromodulatory systems to gate plasticity. The catecholaminergic locus coeruleus (LC) is a major neuromodulatory system involved in neuronal plasticity in the cortex. Using two-photon calcium imaging in mice exploring a virtual environment, we found that the activity of LC axons in the cortex correlated with the magnitude of unsigned visuomotor prediction errors. LC response profiles were similar in both motor and visual cortical areas, indicating that LC axons broadcast prediction errors throughout the dorsal cortex. While imaging calcium activity in layer 2/3 of the primary visual cortex, we found that optogenetic stimulation of LC axons facilitated learning of a stimulus-specific suppression of visual responses during locomotion. This plasticity – induced by minutes of LC axon stimulation – recapitulated the effect of visuomotor learning on a scale that is normally observed during visuomotor development across days. We conclude that prediction errors drive LC activity, and that LC activity facilitates sensorimotor plasticity in the cortex, consistent with a role in modulating learning rates.

**** Dear reader, please note this manuscript is formatted in a standard submission format, and all statistical information is in Table S1. ****

INTRODUCTION

Through experience with the world, brains learn to predict the sensory feedback generated by movement. For instance, learning the precise relationship between motor commands and the resulting visual

feedback is the basis for both feedback control of movements as well as distinguishing self-generated from externally generated sensory feedback. One way that the brain may learn to do this is via predictive processing (Keller and Mrsic-Flogel, 2018; Rao and Ballard, 1999). In a sensorimotor version of this framework, the brain learns an internal model which transforms motor activity into a prediction of the sensory consequences. The framework postulates that specific neurons are responsible for computing discrepancies – known as prediction errors – between the prediction and the actual sensory inputs received. The neocortex has been shown to compute signals consistent with sensorimotor prediction errors (Eliades and Wang, 2008; Keller and Mrsic-Flogel, 2018; Schneider et al., 2018). In the primary visual cortex (V1), excitatory neurons in layer 2/3 compute mismatches between visual flow speed and locomotion speed (Attinger et al., 2017; Jordan and Keller, 2020; Keller et al., 2012; Zmarz and Keller, 2016). Such sensorimotor prediction error responses in the cortex depend on ongoing and developmental experience with sensorimotor coupling (Attinger et al., 2017; Schneider et al., 2018; Vasilevskaya et al., 2022; Widmer et al., 2022), and therefore the computation underlying them is actively learned. In predictive processing, one main function of prediction errors is to drive corrective plasticity in the internal model that generates predictions (Keller and Mrsic-Flogel, 2018).

During the first sensorimotor experience in life, prediction errors should strongly drive learning of an internal model of the world, while later in life, prediction errors should update internal models primarily when overall prediction errors are abundant (for instance, in novel or volatile situations). One way to implement such a developmental or contextual shift in the amount of plasticity induced by a particular prediction error would be a gating signal. The characteristics of a gating signal are that it is activated by prediction errors and that it permits increases in plasticity. In addition, because it is not driving plasticity, but simply gating it, it can be low dimensional (i.e., the same for all neurons). Prime candidates for a gating signal are neuromodulatory systems. Dopaminergic neurons in the midbrain signal reward prediction errors (Kim et al., 2020; Schultz, 2016) and action prediction errors (Greenstreet et al., 2022), which are thought to gate plasticity in downstream targets to support learning of stimulus-reward associations and goal directed behavior (Cox and Witten, 2019; Flagel et al., 2011; Reynolds et al., 2001; Steinberg et al., 2013). Indeed, the catecholamines – dopamine and noradrenaline – regulate and gate plasticity in the cortex (Choi et al., 2005; He et al., 2015; Seol et al., 2007). However, the midbrain dopaminergic system projects only sparsely to most of the sensory neocortex of the mouse, including V1 (Nomura et al., 2014), where visuomotor predictions are thought to be learned (Attinger et al., 2017; Widmer et al., 2022). Instead, the major catecholaminergic input to the cortex is the locus coeruleus (LC). LC activity has

61 primarily been investigated in the context of classical stimulus presentations and reinforcement tasks.
62 Such studies have shown that the LC responds to many different events, including unexpected task
63 outcomes (Bouret and Sara, 2004; Breton-Provencher et al., 2022), novelty (Takeuchi et al., 2016; Vankov
64 et al., 1995), and unexpected sensory stimuli in general (Aston-Jones and Bloom, 1981; Deitcher et al.,
65 2019; Foote et al., 1980; Hervé-Minvielle and Sara, 1995). In zebrafish, noradrenergic neurons increase
66 their activity during the prolonged visuomotor mismatches of failed swim attempts to drive 'giving up'
67 behavior (Mu et al., 2019). We hypothesized that if the mouse LC is activated during similar visuomotor
68 mismatches, this could represent visuomotor prediction error signaling that would function to gate
69 prediction error driven plasticity in output circuits like the cortex.

70 To test fundamental aspects of this idea, we imaged calcium activity in LC axons in the cortex during
71 visuomotor mismatches, and optogenetically manipulated LC activity levels during visuomotor experience
72 to probe for experience dependent changes in cortical activity. We found that LC axons in both sensory
73 and motor cortical regions respond to unsigned visuomotor prediction errors, i.e., unpredicted visual
74 motion or unpredicted visual halts during locomotion. We then combined optogenetic LC axon stimulation
75 with two-photon calcium imaging of layer 2/3 neurons in V1, to show that the LC greatly facilitates a form
76 of plasticity consistent with predictive visuomotor learning: learned suppression of nasotemporal visual
77 flow responses during forward locomotion. These results support the idea that a key function of the LC is
78 to facilitate prediction error driven cortical plasticity.

79 **RESULTS**

80 We first assessed whether locus coeruleus (LC) axons convey sensorimotor prediction errors to the cortex.
81 To record LC axonal activity, we expressed axon-targeted, Cre-dependent GCaMP6s in noradrenergic
82 neurons of the LC via stereotactic viral vector injections in 13 NET-Cre mice (NET = norepinephrine
83 transporter) (Wagatsuma et al., 2018). We confirmed that these injections labelled only cells in the LC,
84 and that GCaMP6s positive cells were also immunoreactive for tyrosine hydroxylase, a marker for
85 catecholaminergic neurons (**Figure S1A**). For two-photon imaging, we implanted a 4 mm imaging window
86 either over the right V1 and surrounding cortical regions (posterior cortex, 9 mice), or over the right
87 primary and secondary motor cortices (anterior cortex, 4 mice). Prior to imaging, mice were habituated
88 to a virtual reality (VR) system consisting of a virtual tunnel, with walls patterned with vertical sinusoidal
89 gratings (**Figure 1A**). In the closed loop condition, locomotion was coupled to visual movement of the

90 tunnel, and in open loop conditions, the walls move independent of mouse locomotion. After habituation
91 to head-fixation, we began imaging across up to five non-overlapping fields of view (FoV) in each imaging
92 window, yielding a total of 31 posterior cortex FoVs and 9 anterior cortex FoVs. Axonal fluorescence
93 showed strong correlations with pupil diameter (**Figure S1B**) typical for LC axons (Reimer et al., 2016),
94 rapid responses to air puffs (**Figure S1C**) as previously reported (Breton-Provencher et al., 2022; Deitcher
95 et al., 2019), and increases in fluorescence at locomotion onset that decayed during the locomotion bout
96 (**Figure S2**) consistent with earlier work (Reimer et al., 2016). We found that within a FoV, individual axon
97 segments exhibited highly correlated activity (**Figures 1B and S1D-F**). Given that the algorithms that
98 identify axons (i.e., determine whether two axon segments belong to the same axon) rely on temporal
99 correlations of activity (Leinweber et al., 2017; Mukamel et al., 2009), axon segmentation is difficult in
100 these data. Thus, to prevent oversampling of the data, we pooled data from all axon segments within a
101 FoV for further analysis.

102 **Locus coeruleus cortical axons signal unsigned visuomotor errors**

103 To determine whether LC axons respond to visuomotor errors, we first measured their responses to
104 visuomotor mismatch stimuli (unexpected 1 s halts of visual flow during locomotion in the closed loop
105 condition). Indeed, LC axons showed significant increases in fluorescence following mismatch
106 presentations (**Figure 1C-D**). Assuming these responses reflect visuomotor prediction errors, we would
107 expect to find two things:

108 First, the responses should depend on precise coupling between visual flow speed and locomotion speed
109 (i.e., when visual flow is predictable from locomotion). Responses to visuomotor mismatch in closed loop
110 conditions should be higher than responses to a replay of the same visual flow halt (termed 'playback
111 halt') in open loop conditions, even when the mouse is locomoting. Playback halts are visually identical to
112 mismatches but occur independent of whether the mouse is stationary or locomoting. Responses of LC
113 axons to playback halts when the mouse was stationary were negative and substantially different from
114 mismatch responses (**Figure 1C-D**), demonstrating that the response of LC axons to visuomotor mismatch
115 cannot be explained by the visual stimulus alone. The mismatch responses also could not be explained by
116 a locomotion driven increase in gain of the visual halt response: a) The average playback halt response
117 when the mouse was stationary was negative, b) there was no correlation between playback halt
118 responses and mismatch responses across different FoVs ($R^2 = 0.04$, $p = 0.31$, 25 FoVs, linear regression),
119 and c) mismatch responses were significantly larger than playback halt responses that occurred during

locomotion in the open loop condition (**Figure 1D**). This indicated that responses in LC axons were acutely dependent on visuomotor coupling, since the only difference between a mismatch stimulus and a playback halt during locomotion is that the former occurs during visuomotor coupling and the latter does not.

Second, the mismatch response should scale with the size of the error between visual flow speed and locomotion speed, since the latter is a proxy for the prediction of visual flow speed. Since visual flow speed is zero during mismatch, and visual flow is perfectly coupled to locomotion prior to mismatch, the visuomotor error is proportional to the locomotion speed during mismatch (**Figure 1A**). Indeed, we found that LC axonal mismatch responses increased monotonically with the locomotion speed of the mouse (**Figure 1E**). Thus, LC axonal responses to visuomotor mismatch are consistent with a visuomotor prediction error signal.

Visuomotor mismatches evoke negative prediction errors because they are a condition where there is *less* visual flow than expected. However, these are not the only type of prediction error in our paradigm. In the open loop condition, visual flow onsets result in positive prediction errors (i.e., a condition with *more* visual flow than expected), especially when the mouse is stationary. We thus assessed the responses of LC axons to visual flow onsets in the open loop condition (i.e., not coupled to locomotion). We found that LC axons showed significant responses to visual flow onsets, but only when the mouse was stationary (**Figure 1F-G**). Visual flow onsets during locomotion did not evoke significant responses on average. Altogether, LC axonal responsiveness to visual and visuomotor stimuli was best explained by the absolute (i.e., unsigned) error between locomotion and visual flow speeds ($|Error| = |Speed_{locomotion} - Speed_{visual\ flow}|$). Changes in the absolute error resulted in corresponding changes in the activity in LC axons (**Figures 1C and 1F**), and responses scaled with the size of $\Delta|Error|$ (i.e., the change in unsigned error magnitude, see Methods) across the different stimulus conditions (**Figure 1H**).

Noradrenaline broadcasts visuomotor prediction errors across the dorsal cortex

Individual LC neurons can preferentially target different cortical areas (Chandler et al., 2019; Kebschull et al., 2016), but it is unclear whether these projection-specific neurons have differing response profiles. To assess the heterogeneity of LC signaling across the cortex, we first compared the calcium responses of LC axons between two imaging window locations: the anterior cortex (the primary and secondary motor cortex), and the posterior cortex (V1 and surrounding regions) (**Figure 2A**). We found very similar responses to visuomotor mismatches, playback halts (stationary) and visual flow onsets (stationary)

150 (**Figure 2B**), as well as air puffs and locomotion onsets at these two locations (**Figure 2C**), and there were
151 no significant differences in the responses between the two locations. These results are consistent with
152 the idea that the LC sends the same visuomotor and locomotion related signals to distinct regions of the
153 cortex, in line with recent findings showing that LC axons in different cortical regions show responses to
154 the same sensory stimuli (Deitcher et al., 2019).

155 **We find no evidence of an effect of locus coeruleus axon stimulation on average responses in layer 2/3**
156 **of V1**

157 What could be the function of prediction errors signaled by the LC to the cortex? One possibility is that
158 cortical prediction errors, like mismatch responses in V1 (Keller et al., 2012), are enhanced by LC output
159 in order to augment error driven learning. Indeed, a prevalent idea is that noradrenaline is a mediator of
160 gain modulation in the cortex (Ferguson and Cardin, 2020), including the gain increase in V1 during
161 locomotion (Polack et al., 2013). To test whether the LC may enhance prediction error responses in cortical
162 layer 2/3, we assessed the impact of transient LC axon stimulation on cortical responses using an
163 optogenetic strategy (**Figure 3A**). First, we injected an AAV vector encoding Cre-dependent excitatory red-
164 light activated opsin, ChrimsonR, into the right LC of 8 NET-Cre mice, while injecting a vector encoding
165 jGCaMP8m into the right V1 to drive non-specific neuronal expression. An imaging window was then
166 implanted over the right V1. Mice underwent habituation to the virtual reality system before calcium
167 imaging of V1 neurons during 1) a closed loop condition with mismatches and 2) an open loop condition
168 with 1 s fixed-speed visual flow stimuli. During imaging, we stimulated ChrimsonR by directing a 637 nm
169 laser through the objective onto the craniotomy (27 mW/mm^2, in 15 ms pulses presented at 20 Hz). This
170 stimulation was presented a) alone in closed loop conditions, b) coupled to a random 50% of mismatches
171 (**Figure 3B**), and c) coupled to a random 50% of open loop visual flow stimuli. To assess the visual effects
172 of optical stimulation of ChrimsonR (Danskin et al., 2015) in absence of the effects of optogenetically
173 stimulating LC axons, we also imaged from a second group of 6 mice treated in an identical manner, but
174 without ChrimsonR expression in the LC (control mice). Two mice were excluded from the LC-injected
175 group due to low density of axonal labelling with tdTomato in V1, leaving 6 ChrimsonR-expressing mice in
176 the dataset (see Methods).

177 Optogenetic stimulation, when presented in isolation, resulted in dilations of the right pupil in mice
178 expressing ChrimsonR (**Figure 3C**), but not in control mice. This potentially resulted from antidromic
179 activation of the LC, direct stimulation of which is known to produce strong ipsilateral pupil dilation (Liu

180 et al., 2017), and increased our confidence that we were indeed driving LC axons with the parameters
181 selected. Onset of the optogenetic stimulation laser caused a small calcium response across the
182 population in ChrimsonR-expressing mice, which was indistinguishable from that caused in control mice
183 (**Figure 3D**). This was likely due to a visual effect of the stimulation laser. The lack of a difference in this
184 stimulation response between ChrimsonR-expressing mice and control mice indicated that optogenetic
185 stimulation of LC axons did not have a direct measurable effect on calcium activity of L2/3 neurons in V1.

186 We then analyzed the effect of optogenetic activation of LC axons on stimulus responses of the layer 2/3
187 population. Stimulation of ChrimsonR in LC axons had no significant effect on average visuomotor
188 mismatch responses of layer 2/3 neurons, and the difference in response size compared between trials
189 with and without laser stimulation was indistinguishable from that seen in control mice (**Figure 3E**). The
190 same was true for visual flow responses (**Figure 3F**). The only observable difference in responses during
191 optogenetic stimulation was that responses to visual flow onsets (i.e., at the beginning of the visual flow
192 stimulus, or at the offset of mismatch) appeared slightly more pronounced (**Figure 3E-F**).

193 In V1, there is electrophysiological and molecular evidence for at least three different layer 2/3 pyramidal
194 neuron types, including negative prediction error (NPE) neurons which respond to visuomotor
195 mismatches, positive prediction error neurons (PPE) which respond to unexpected visual flow (Jordan and
196 Keller, 2020; O'Toole et al., 2022), and an intermediate group. It is therefore conceivable that LC output
197 could have differential effects on these groups that are masked when analyzed at the population level. To
198 quantify potential cell-type specific effects of LC axon stimulation, we thus split the population of neurons
199 into three groups based on locomotion onset responses (see **Figure S3** and Methods): the group with the
200 strongest visuomotor mismatch responses (NPE), the group with the strongest visual flow responses
201 (PPE), and an intermediate population (Other) (**Figure S3**). We found no evidence for an effect of
202 optogenetic stimulation of LC axons on average mismatch and visual flow responses across any of these
203 cell groups (**Figure 3G-H**). We thus concluded that transient LC axon stimulation in the awake state has
204 only a minor direct effect on the responses of neurons in layer 2/3 of V1.

205 **Phasic LC output enhances sensorimotor plasticity in layer 2/3 of V1**

206 If transient LC activity in the awake state does not overtly affect average layer 2/3 responses directly, what
207 is the function of visuomotor prediction errors signaled by the LC in the cortex? The LC is thought to be
208 involved in cortical plasticity (Kasamatsu et al., 1985; Kasamatsu and Pettigrew, 1976; Martins and
209 Froemke, 2015; Shepard et al., 2015). Catecholamine receptors in V1 are known to modulate synaptic

210 plasticity by activating intracellular signaling cascades and interacting with eligibility traces (Choi et al.,
211 2005; He et al., 2015; Nomura et al., 2014; Seol et al., 2007). One plausible function of LC sensorimotor
212 prediction errors is to gate the plasticity that underlies learning of sensorimotor predictions, e.g., the
213 prediction of visual feedback during locomotion. Primary sensory cortices can indeed learn to suppress
214 the sensory consequences of locomotion, driving selective reductions of responses to locomotion-coupled
215 inputs (Schneider et al., 2018; Widmer et al., 2022).

216 While our optogenetic stimulation of LC axons had no measurable effects on mismatch or visual flow
217 response size (**Figure 3**), we did notice one striking difference between ChrimsonR-expressing and control
218 mice. In V1, there is a known increase in the size of visual responses during locomotion compared to
219 stationary periods (Bennett et al., 2013; Erisken et al., 2014; Niell and Stryker, 2010; Pakan et al., 2016;
220 Polack et al., 2013; Zmarz and Keller, 2016). Analyzing only trials where the optogenetic stimulation laser
221 was not on, we found that this canonical gain increase was present for control mice but reversed in sign
222 in ChrimsonR-expressing mice: Visual responses during locomotion were suppressed on average relative
223 to stationary periods (**Figure 3I**). This resulted in a significantly lower locomotion modulation index (see
224 Methods) for ChrimsonR-expressing relative to control mice (**Figure 3I**). Since episodic LC axon stimulation
225 occurred throughout the whole imaging session (i.e., across 10 minutes in the closed loop condition, prior
226 to the presentation of open loop visual flow stimuli), it is possible that the reversal of locomotion
227 modulation index reflects a result of plasticity induced by earlier LC axon stimulation.

228 We wanted to directly test the idea that transient LC activation enhances plasticity that leads to a
229 reduction in locomotion modulation index over the course of visuomotor coupling experience. To do this,
230 we designed an experiment to assess the impact of LC axon stimulation on neuronal learning about
231 visuomotor coupling (**Figure 4A**). We expressed jGCaMP8m in neurons in V1 of 19 mice. 12 mice also had
232 AAV vector injections into the LC to express ChrimsonR in NET-positive neurons, while the remaining 7
233 underwent no injection into the LC to serve as controls for the non-optogenetic effects of the protocol.
234 Mice were habituated to the VR as before and we then proceeded to two-photon imaging in layer 2/3 of
235 V1. During the imaging session, mice would first be exposed to 5 minutes of 1 s fixed-speed open loop
236 visual flow presentations, to quantify the gain-change of visual flow responses during locomotion (**Figure**
237 **4A**). Mice were then exposed for 5-10 minutes to either a) a closed loop condition where visual flow and
238 locomotion are coupled, or b) an open loop replay of visual flow generated from a previous closed loop
239 session. During this session, LC axons would be periodically optogenetically stimulated as before (15 ms

240 pulses, presented at 20 Hz for 1 s every 7 seconds on average) to simulate phasic LC prediction error
241 responses (**Figure 4A**). Afterwards, the open loop visual flow presentations would be repeated to quantify
242 how the previous LC axon stimulation affected visual responses. To assess the stimulus specificity with
243 which visual responses changed, we presented both nasotemporal and temporonasal visual flow (mice
244 see the former during forward locomotion in the closed loop condition) (**Figure 4A**). If LC axon stimulation
245 results in enhanced plasticity of the internal model that underlies locomotion based predictions of visual
246 flow, we would expect the following observations: 1) Suppression of visual flow responses by locomotion
247 is enhanced after stimulation of LC axons in closed loop conditions, 2) this suppression is specific to the
248 type of visual flow seen during forward locomotion (nasotemporal), 3) the effect depends on ChrimsonR
249 expression in the LC, and 4) the effect is absent when LC axons are instead stimulated during open loop
250 conditions (i.e., the effect depends on visuomotor coupling).

251 Optogenetic stimulation caused a degree of pupil dilation that was strongly predictable from axonal
252 ChrimsonR expression levels in V1 quantified postmortem ($R^2 = 0.89$, $p < 10^{-5}$, 12 mice, linear regression)
253 (**Figure 4B**). We split the LC-injected dataset into high ChrimsonR expression (six mice) and low ChrimsonR
254 expression (six mice) according to V1 axonal expression level (**Figures 4B and S4A**). Low ChrimsonR-
255 expressing mice had optogenetically evoked pupil dilations that were not statistically distinguishable from
256 controls, while high ChrimsonR-expressing mice had overt pupil dilations (**Figures 4B and S4B**). For the
257 following analyses, we excluded 8 (5) of 49 (25) sessions from the ChrimsonR (control) dataset due to lack
258 of locomotion during those sessions (see Methods). At the beginning of the imaging session, prior to
259 optogenetic stimulation, neurons in layer 2/3 showed a pronounced positive locomotion modulation
260 index for both the nasotemporal and temporonasal visual flow responses, both in high and low
261 ChrimsonR-expressing mice and in control mice (**Figures 4C-E and S4D**). Quantifying visual flow responses
262 in high ChrimsonR-expressing mice after optogenetic stimulation during closed loop visuomotor
263 experience revealed a reduction in the locomotion modulation index for nasotemporal visual flow
264 responses (**Figure 4C**). This originated from a reduction in the response to visual flow during locomotion,
265 while responses during stationary periods remained stable (**Figure 4G**). This effect was specific to the
266 direction of visual flow seen during forward locomotion, since locomotion modulation index was
267 preserved for temporonasal visual flow responses (**Figure 4D**), with negligible changes in response size
268 both during locomotion and stationary periods (**Figure 4H**). The effect was also specific to high ChrimsonR-
269 expressing mice, as locomotion modulation index was largely preserved in both control and low
270 ChrimsonR-expressing mice (**Figures 4E, 4I, and S4D**).

271 The selective reduction in locomotion modulation index of nasotemporal visual flow responses in high
272 ChrimsonR-expressing mice could be due to enhanced learning to suppress reafferent visual feedback
273 seen during forward locomotion, or it could simply be due to general exposure to nasotemporal visual
274 flow during optogenetic stimulation (e.g., enhanced adaptation). In the latter case, response size
275 reduction should be the same if optogenetic stimulation takes place during open loop replay of the same
276 visual flow seen during closed loop conditions. To assess this, we repeated the same experiment, but
277 instead of stimulating LC axons during the closed loop condition, we stimulated LC axons during open loop
278 replays of visual flow from previous closed loop sessions of the same mice (**Figure 4A**). Instead of a
279 stimulus selective reduction in locomotion gain, this paradigm drove a nonsignificant increase in
280 locomotion modulation index for both nasotemporal (**Figures 4F and S4F**) and temporonasal visual flow
281 (**Figure S4E**) responses. This confirmed that the reduction in locomotion modulation index after
282 stimulation of LC axons in the closed loop condition (**Figure 4C**) depends on visuomotor coupling
283 experience and is not simply due to exposure to nasotemporal visual flow.

284 We conclude that LC axon stimulation over the course of minutes increases locomotion driven
285 suppression of visual flow responses in layer 2/3 in a manner that is specific to reafferent stimulus
286 properties and dependent on both ChrimsonR expression and visuomotor coupling (**Figure 4J**).
287 Importantly, the effect could not be explained by differences in locomotion behavior between any of the
288 groups analyzed (**Figure S5**).

289 **LC axon stimulation over minutes recapitulates visuomotor plasticity seen over days**

290 In the virtual reality environment, mouse movement and visual flow are constrained to the forward-
291 backward dimension, and the visuomotor gain is constant: changes in visuomotor gain that would usually
292 occur during changes in environment geometry are absent. Mice head-fixed in the VR therefore
293 experience a vastly reduced diversity of visuomotor coupling compared to freely moving conditions. The
294 reduction in locomotion modulation index resulting from LC axon stimulation (**Figure 4C**) may therefore
295 result from overlearning of this simplified visuomotor coupling.

296 If this interpretation is correct, then extensive training within the VR should also lead to visual flow
297 response suppression during locomotion even in mice without artificial LC axon stimulation. To assess this
298 idea, we reanalyzed two-photon calcium imaging data from V1 layer 2/3 in coupled trained mice reared
299 with visual experience entirely constrained to that of the visuomotor coupling in the VR across days (and
300 otherwise dark reared) (Attinger et al., 2017; Widmer et al., 2022) (**Figure 5A**). We compared this data to

301 similar data from normally reared mice that also have experience of the virtual reality system, but that
302 had experience of normal visuomotor coupling in freely moving conditions (Vasilevskaya et al., 2022;
303 Zmarz and Keller, 2016) (**Figure 5A**). Analyzing responses to nasotemporal visual flow onsets during open
304 loop replay, we found that visual flow responses were amplified during locomotion relative to stationary
305 periods in normally reared mice but were suppressed during locomotion in coupled trained mice (**Figure**
306 **5B**). This resulted in a significantly lower locomotion modulation index in coupled trained mice compared
307 to normally reared mice (**Figure 5C**). The effect was not due to dark rearing, as non-coupled trained mice
308 (also dark reared, but with only open loop virtual reality experience (**Figure 5A**) (Attinger et al., 2017))
309 showed a positive locomotion modulation index on average that did not significantly differ from that of
310 normally reared mice (**Figure 5C**).

311 Qualitatively, the comparison of locomotion modulation index between normally reared and coupled
312 trained mice (**Figure 5B-C**) was similar to the change in locomotion modulation index in ChrimsonR-
313 expressing mice for nasotemporal visual flow after LC axon stimulation (**Figure 4C**). This suggests that the
314 increase in locomotion driven suppression after LC axon stimulation is caused by a similar form of plasticity
315 to that seen when visuomotor experience is constrained to the virtual reality across days. If this is the
316 case, we should see similarities in the properties of the locomotion driven suppression. First, we looked
317 at the locomotion speed dependence of the suppression. If the negative locomotion modulation index
318 results from learning to suppress visual responses according to a locomotion driven prediction of visual
319 flow, the degree of suppression should depend on locomotion speed. As locomotion speed increased,
320 visual flow responses were increasingly suppressed in coupled trained mice (**Figure 5D**), while this was
321 not evident in normally reared mice (**Figure 5E**). For nasotemporal visual flow responses in ChrimsonR-
322 expressing mice, locomotion modulation index was positive and did not change with locomotion speed at
323 the start of the imaging session, but after stimulation of LC axons in closed loop conditions, locomotion
324 modulation index became increasingly negative as locomotion speed increased (**Figure 5F-G**). Thus, the
325 locomotion driven suppression of visual flow emerging after stimulating LC axons in closed loop conditions
326 was locomotion speed dependent in a similar manner to the locomotion driven suppression seen in
327 coupled trained mice. Note that in high ChrimsonR-expressing mice, suppression of visual flow was seen
328 at high locomotion speeds only (**Figure 5G**), but in coupled trained mice, some level of suppression was
329 evident across all speeds (**Figure 5E**). This could be due to differences in visual flow speed: for coupled
330 trained mice, the stimuli analyzed are visual flow onsets during open loop replay; thus, the visual flow
331 speed will cover a similar range as the locomotion speed distribution of the mice. For high ChrimsonR-

332 expressing mice, the stimuli are presented at a fixed visual flow speed that often exceeds the locomotion
333 speed of the mouse. Thus, the fact that suppression only appears at the highest locomotion speed in these
334 mice is consistent with a suppression of visual flow input based on a locomotion speed dependent
335 expectation. In addition to the similarities in locomotion speed dependence of suppression in the two
336 groups, the pattern of change in locomotion modulation index across different functional layer 2/3 cell
337 groups also appeared similar between high ChrimsonR-expressing and coupled trained mice (**Figure S6**).

338 Overall, the pattern of differences in locomotion modulation was remarkably similar for ChrimsonR-
339 expressing (**Figures 5G, and S6D**) and coupled trained mice (**Figures 5E and S6B**). This indicates that
340 functional consequences of the plasticity evoked by 5-10 minutes of LC axon stimulation during
341 visuomotor coupling, and that seen over the course of several days of experience being constrained to
342 visuomotor coupling in the virtual reality, are similar.

343 DISCUSSION

344 The locus coeruleus (LC) has long been hypothesized by computational models to report quantities such
345 as unexpected uncertainty (Yu and Dayan, 2005) or high level state-action prediction errors (Sales et al.,
346 2019). What these quantities have in common is that they essentially are metrics for the inaccuracy of the
347 brain's internal models. One way to implement such a measure would be to integrate prediction errors
348 from across the brain and then broadcast this signal back across the brain. Indeed, we found that the LC
349 sends unsigned visuomotor prediction errors non-specifically across the dorsal cortex (**Figures 1 and 2**).
350 Models hypothesizing that the LC reports the global inaccuracy of the brain's internal models suggest that
351 the purpose of this is to increase learning rates in output circuits like the cortex, enabling internal models
352 to be modified more rapidly. In line with this, we found that stimulating cortical LC axons during closed
353 loop visuomotor coupling over minutes reduces and even reverses the canonical locomotion related gain
354 of visual flow responses in layer 2/3 of V1, in a manner specific to the direction of the movement-coupled
355 stimulus (**Figure 4**). Surprisingly, this enhanced plasticity seems to happen even with no overt direct effect
356 of LC axon stimulation on average calcium responses (**Figure 3**). This plasticity, on the timescale of
357 minutes, recapitulates the effect of restricting visuomotor experience to the closed loop coupling in virtual
358 reality across days (**Figure 5**), suggesting that it reflects an acceleration of a slower form of visuomotor
359 plasticity (i.e., an increased learning rate).

360 The LC responds to unexpected stimuli of various modality, including reward prediction errors, and novel
361 or intense unexpected sensory stimuli (Aston-Jones and Bloom, 1981; Bouret and Sara, 2004; Breton-
362 Provencher et al., 2022; Deitcher et al., 2019; Foote et al., 1980; Hervé-Minvielle and Sara, 1995; Takeuchi
363 et al., 2016; Vankov et al., 1995). The responses we found here in LC axons to the various visual flow
364 stimuli were proportional to the change in the degree of error between visual flow and locomotion speeds
365 (**Figure 1**). This supports a model in which the LC signals prediction errors, and combined with previous
366 findings, suggests that prediction errors of all modalities are a general feature of LC signaling. Based on
367 the multimodality and unsigned nature of LC responses, and the integrate and broadcast nature of its
368 input-output anatomy (Schwarz et al., 2015), our working model of LC function is as follows: The LC
369 integrates prediction errors of all modalities to compute a measure of how inaccurately internal models
370 are currently predicting the global sensory inputs of the animal. The LC does not signal what *type* of
371 prediction error occurred, but what the global rate of prediction errors currently is (i.e., a measure of
372 surprise). The resulting LC output does not directly *drive* model updating in cortical output areas, but it
373 modulates the rate at which local cortical prediction errors drive plasticity in internal models. Thus, the
374 specificity of how internal models are changed depends on ongoing prediction errors in the cortex, and
375 the LC input acts to control the learning rate, modulating the extent to which these cortical prediction
376 errors drive plasticity. This would allow the LC to be a controller of plasticity in internal models: when
377 prediction error rates are high (i.e., during developmental, novel, or volatile situations), updating of
378 internal models will be more rapid as a result of increased LC output.

379 While the idea of a brain wide average over sensory prediction errors can explain many of the observed
380 LC responses, other responses are less easily explained by prediction error. LC calcium responses to
381 locomotion onsets, which have been shown previously in LC axons (Deitcher et al., 2019; Reimer et al.,
382 2016), were generally larger than visual flow or visuomotor mismatch responses (**Figures 2 and S2**). This
383 could be the result of a direct movement related input unrelated to prediction errors, or the result of
384 prediction errors that are not driven by differences between forward locomotion and backward visual
385 flow. Increases in activity occurring after locomotion onset could reflect vestibulomotor prediction errors
386 that result from the fact that the mouse is head-fixed, or visuomotor prediction errors for motor attempts
387 we do not record, like turns or head movements. We do find that visuomotor prediction errors contribute
388 to locomotion onset responses, as locomotion onset responses in the open loop condition are smaller
389 during visual flow, when locomotion evoked visuomotor error is lower (**Figure S2B**). However, LC calcium
390 activity also rises prior to locomotion onset, creating the additional possibility of an internally generated

391 movement onset response. Other kinds of movement are also correlated with LC firing, including pup
392 retrievals (Dvorkin and Shea, 2022) and lever pressing (Breton-Provencher et al., 2022). These movement
393 onset responses could also reflect other forms of prediction error, including action prediction errors
394 (Greenstreet et al., 2022) or temporal difference reward prediction errors (in cases where the movement
395 is associated with reward expectation) similar to those documented in the dopaminergic system (Kim et
396 al., 2020). Future work will need to investigate these possibilities to build a complete general model of LC
397 computation.

398 Depleting noradrenaline has been shown to prevent forms of sensory-guided developmental plasticity in
399 the cortex, including ocular dominance plasticity in V1 (Kasamatsu and Pettigrew, 1976) and changes in
400 the tonotopic map in the auditory cortex (Shepard et al., 2015). Loss of function experiments can suffer
401 from the potential confound that catecholamines may simply be necessary for normal neuronal activity,
402 and the loss of plasticity may be a secondary effect of a disruption in neuronal function. Indeed, acute
403 noradrenergic receptor block can silence neurons in layer 2/3, and massively reduce the amplitude of
404 visual inputs (Polack et al., 2013). In gain of function experiments, electrical stimulation of the LC has been
405 shown to partially restore ocular dominance plasticity in adult cats (Kasamatsu et al., 1985). Here we also
406 performed a gain of function experiment: we show that a few minutes of optogenetic LC axon stimulation
407 in V1 of adult mice during visuomotor coupling can recapitulate the developmental effects of constrained
408 exposure to visuomotor coupling in the virtual reality (**Figure 4 and 5**). While our optogenetic stimulation
409 is likely far more constrained to LC neurons than previous electrical stimulations, we cannot rule out a
410 systemic effect of the LC axon stimulation. We know that we are likely antidromically activating the LC
411 with our optogenetic stimulation owing to the resulting pupil dilation (**Figures 3C and 4B**). Given that LC
412 neurons are electrically coupled (McKinney et al., 2022) and have widely divergent axons, our stimulation
413 likely has effects on other LC output targets, such as other neuromodulatory systems, and other areas of
414 the cortex. Thus, the plasticity effect that we measure may not entirely result from LC output in V1 alone.
415 However, since the LC will never be acting in isolation and broadcasts its output to different cortical areas,
416 the functional impact of LC axon stimulation in this experiment is strongly suggestive of a role in facilitating
417 plasticity. Future work will be needed to understand the circuit locus of plasticity generated by this
418 paradigm, and its dependence on particular neuromodulators (e.g., dopamine and noradrenaline).

419 Prediction error driven catecholamine release is thought to gate cortical synaptic plasticity during
420 reinforcement learning (He et al., 2015; Roelfsema and Holtmaat, 2018). The results presented here

421 expand this idea from reward associations to sensorimotor associations. We propose that a general
422 function of catecholamines is to gate the plasticity underlying predictive learning across all modalities.

423 AUTHOR CONTRIBUTIONS

424 RJ designed and performed the experiments and analyzed the data. Both authors wrote the manuscript.

425 ACKNOWLEDGEMENTS

426 We thank all members of the Keller lab for discussion and support, Tingjia Lu for the production of viral
427 vectors, Susumu Tonegawa for sharing NET-Cre mice, and Andreas Lüthi for reagents and equipment. This
428 project has received funding from Human Frontier Science Program (LT000077/2019-L, long term
429 fellowship to RJ), the Swiss National Science Foundation, the Novartis Research Foundation, and the
430 European Research Council (ERC) under the European Union's Horizon 2020 research and innovation
431 programme (grant agreement no. 865617).

432 DATA AND CODE AVAILABILITY.

433 All data and analysis code are available at https://data.fmi.ch/PublicationSupplementRepo/.

434 METHODS

435 **Viral vector injections and surgery.** All animal procedures were approved by and carried out in
436 accordance with guidelines of the Veterinary Department of the Canton Basel-Stadt, Switzerland. For all
437 surgical procedures, mice were anesthetized with an intraperitoneal injection of a mixture of fentanyl
438 (0.05 mg/kg), medetomidine (0.5 mg/kg), and midazolam (5 mg/kg) and provided with both peri- and
439 postoperative general and local analgesics: Metacam (5mg/kg, s.c.) and buprenorphine (0.1 mg/kg, s.c.).
440 A lidocaine and ropivacaine mixture was injected subcutaneously into the scalp prior to incision. Metacam
441 analgesia was provided for a further 48 hours post-surgery. Mice were allowed to recover for 1-3 weeks
442 prior to first head-fixation.

443 **Surgeries for two-photon imaging of LC axons.** 13 male and female NET-Cre (Wagatsuma et al., 2018)
444 mice (4-6 weeks old) were unilaterally injected at stereotactic coordinates (relative to bregma and brain
445 surface): 5.45 mm posterior, 1.10 mm lateral, 3.65 mm deep. 250 to 500 nl of AAV2/5-hSyn-DIO-axon-
446 GCaMP6s (2.7 x 10^{13} genome copies/ml) was injected into each site. A 4 mm diameter circular imaging

447 window was then implanted. A circular craniotomy was made overlying visual cortex (8 mice) or motor
448 cortex (4 mice) and a durectomy was performed. A glass window was then placed onto the craniotomy
449 and fixed in place with cyanoacrylate. A custom titanium headplate was attached to the skull using dental
450 cement (Paladur, Kulzer).

451 **Surgeries for two-photon imaging in layer 2/3 V1 during optogenetic stimulation of LC axons.** Male and
452 female NET-Cre mice (4-6 weeks old) were unilaterally injected with 250 to 500 nl of AAV2/1-hSyn-DIO-
453 ChrimsonR-tdTomato (1.2 x 10^{13} to 3.4 x 10^{13} genome copies/ml) into the right LC at stereotactic
454 coordinates (relative to bregma and brain surface): 5.45 mm posterior, 1.10 mm lateral, 3.65 mm deep. A
455 maximum of 250 nl of AAV2/1-hSyn-soma-jGCaMP8m (titer range from 10^{13} to 10^{15} genome copies/ml)
456 was then injected across 3-5 locations spanning right V1, and a window and headplate were implanted as
457 above, but with the additional measure of black pigmenting of the dental cement for the reduction of
458 optogenetic stimulation light reaching the eyes of the mouse. For control mice, the injection into the LC
459 was omitted. For the dataset in **Figure 3**, eight mice were injected in the LC, but two were excluded due
460 to lack of expression (see section Axon density). Six mice were not injected in the LC to serve as controls.
461 For the dataset in **Figure 4**, 12 mice were injected in the LC, with 6 mice classified as high ChrimsonR
462 expression and 6 classified as low ChrimsonR expression (see section Axon Density). 7 mice were not
463 injected in the LC to serve as controls.

464 **Immunohistochemistry**. For all experiments with vector injections in LC to express either GCaMP or
465 ChrimsonR-tdTomato, we histologically verified that expression was confined to the neurons within the
466 anatomical location and spatial pattern expected of the LC. In a subset of mice used for imaging LC axons,
467 we also confirmed that the transgene expressing neurons were catecholaminergic by immunostaining for
468 tyrosine hydroxylase and GFP (**Figure S1A**). After transcardial perfusion, brains were extracted and placed
469 in 4% paraformaldehyde overnight. Brains were then embedded in 4% agar and sliced at 40 µm on a
470 vibratome. Free floating slices were then washed in PBS-triton, blocked for 2 hours with 10% goat serum,
471 and incubated overnight with primary antibodies (1:1000 dilution rabbit anti-tyrosine hydroxylase (Abcam
472 ab13970), and 1:500 dilution chicken anti-GFP (Abcam ab13970). The following day, slices were washed
473 again in PBS-triton and incubated for 2 hours with the secondary antibodies at 1:1000 dilution (Alexa Fluor
474 488 anti-chicken (Jackson ImmunoResearch 703-545-155) and Alexa Fluor 568 anti-rabbit (ThermoFisher
475 Scientific, A10042)). Slices were mounted in Fluoroshield with DAPI (F6057, Sigma Aldrich).

476 **Virtual reality and visual stimuli.** A virtual tunnel, with walls patterned with vertical sinusoidal gratings
477 was projected onto a toroidal screen spanning 240 degrees horizontally and 100 degrees vertically of the
478 visual field. The projector output was gated by a 24 kHz TTL such that it only turned on at the turnaround
479 points of the two-photon resonance scanner, minimizing light artifacts during imaging. Mice were head-
480 fixed on an air-floated polystyrene ball of 20 cm diameter. Movement of the virtual tunnel walls could
481 occur only in one dimension (forward and backwards), with the ball restricted to rotation around the pitch
482 axis using a pin. In closed loop conditions, visual flow speed in the tunnel was coupled to the rotation of
483 the ball, with the exception of brief 1 s mismatch stimuli. These were triggered every 12 ± 2 s (mean ± SD)
484 regardless of locomotion behavior and would clamp the visual flow speed to zero. In open loop conditions,
485 the visual flow speed was controlled irrespective of mouse locomotion. Three different types of open loop
486 session were used: 1) for LC axon imaging (**Figures 1 and 2**), as well as optogenetic stimulation of LC axons
487 during open loop replays (**Figure 4**), the visual flow from a previous closed loop session would be replayed.
488 For LC axon imaging, the visual flow onset responses and playback halt responses were analyzed during
489 this session. 2) For stimulation of LC axons to assess the effect on cortical responses (**Figure 3**), 1 s fixed
490 speed nasotemporal visual flow stimuli would be presented every 9 ± 3 s (mean ± SD). We presented 3
491 different speeds of visual flow in a pseudorandom order. 3) For assessing the effects of LC axon stimulation
492 on visuomotor plasticity (**Figure 4**), we presented 1 s duration fixed speed visual flow stimuli every 7 ± 1 s
493 (mean ± SD), but this time only one speed was presented (equivalent to the speed seen during 24 cm/s
494 locomotion in closed loop conditions), however, the direction was either nasotemporal or temporonasal,
495 in a pseudorandom order. All mice imaged were habituated to head-fixation and the virtual reality tunnel
496 for at least four daily one-hour sessions prior to imaging, until they showed regular, comfortable
497 locomotion.

498 **Two-photon imaging.** Imaging was performed on a modified Thorlabs Bergamo II two-photon microscope
499 system. Excitation illumination was provided by a Ti-Sapphire laser with a wavelength at 930 nm and a
500 laser power between 20 and 30 mW under the objective. When imaging neurons in V1, a piezo scanner
501 was used to move the objective to image 4 separate layers sequentially (15 Hz effective frame rate), but
502 for LC axons, imaging was fixed in a single layer (60 Hz frame rate). Field of view size was 750 × 400 pixels
503 (approximately 300 x 300 µm). Custom software was used to acquire the imaging data. For mice
504 undergoing imaging of layer 2/3 V1 neurons (**Figures 3 and 4**), two-photon imaging sites were confirmed
505 as being in V1 by mapping V1 boundaries using intrinsic signal optical imaging.

506 **Optogenetic stimulation of LC axons.** The beam from a 637 nm OBIS laser (Coherent) was focused onto
507 the imaging site via the two-photon microscope objective. The laser was gated to turn on only during the
508 turnaround times of the two-photon resonance scanner, to minimize stimulation induced light artifacts.
509 During stimulation, the laser was presented in 15 ms pulses at 20 Hz (30% duty cycle) for a total duration
510 of 1 s. For stimulation during visual stimulus presentations (**Figure 3**), the power was 27 mW/mm^2. Since
511 this evoked a small visual response in the V1 calcium activity of both ChrimsonR-expressing and control
512 mice (**Figure 3C**), the power was reduced for subsequent experiments to 20 mW/mm^2 (**Figure 4**), at which
513 point the positive visual response disappeared (**Figure S4C**). For the optogenetic stimulation during visual
514 stimulus presentations (**Figure 3**), optogenetic stimulation occurred simultaneous with a random 50% of
515 mismatch stimuli and visual flow stimuli, or in isolation, every 12 s on average, during closed loop
516 conditions. For optogenetic stimulation in the plasticity experiments (**Figure 4**), stimulation occurred
517 every 7 s on average. In 17/61 included imaging sites, this was gated by mouse locomotion such that
518 stimulation only occurred when locomotion speed exceeded 4 cm/s. Since the results looked very similar
519 for both locomotion gated and ungated stimulations, the data were pooled for analysis.

520 **ΔF/F calculation.** Raw images were full-frame registered to correct for lateral brain motion. For V1 layer
521 2/3 neurons, neuronal somata were manually selected based on mean and maximum fluorescence
522 images. Average fluorescence per region of interest (ROI) was corrected for slow fluorescence drift over
523 time using an 8th percentile filter and a 1000 frame window, and divided by the median value over the
524 entire trace to calculate ΔF/F (Dombeck et al., 2007). For LC axonal data (**Figures 1 and 2**), there were a
525 number of alternative/additional steps. First, all ROIs within an image above a manually set fluorescence
526 threshold were selected. Non-axonal ROIs from this set were then removed in two ways: first, a 'circularity
527 index' (circularity index = 4π x $area/perimeter^2$) and area threshold were used. ROIs with circularity index
528 above 0.14 or a total area below 150 pixels were excluded – this served to remove non-axonal structures.
529 Second, any ROI without evidence of calcium activity was removed: a fast Fourier transform was used to
530 obtain the power spectrum of the ΔF/F trace. From this, the signal-to-noise ratio of the calcium signal was
531 calculated, where noise was calculated as the average power between 3 and 8 Hz. ROIs with power below
532 a signal-to-noise ratio of 10 in the frequency band from 0.05 to 1 Hz (classified as signal) were excluded.
533 This served to remove uncommon elongated non-axonal ROIs, such as blood vessel walls. Next, due to the
534 lower signal to noise of the axonal recordings, the ΔF/F recorded at 60 Hz was low pass filtered at 10 Hz.
535 Finally, due to the high correlation of ΔF/F between LC axonal ROIs within a field of view (**Figure S1D-F**),
536 ΔF/F was averaged across all axonal ROIs within a field of view.

537 **Calculation of visuomotor error (Figure 1).** Visuomotor error is calculated as the difference between
538 locomotion speed and visual flow speed, assuming a constant gain between that the two the mouse
539 predominantly experiences in the virtual reality. The change in absolute error (Δ|Error|) is calculated for
540 each trial as the change in absolute (i.e., unsigned) visuomotor error during the stimulus window, minus
541 the absolute visuomotor error in the 1 s preceding the stimulus. For each type of stimulus and each FoV,
542 Δ|Error| was then averaged across trials. Note that for visuomotor mismatch, Δ|Error| is equivalent to
543 the locomotion speed during mismatch (since visual flow speed during mismatch is zero, and the
544 preceding 1 s is closed loop, where the error is zero). In all stimulus conditions (**Figure 1H**), the Δ|Error|
545 is calculated in a window 0.66 s (40 frames) preceding the window used to calculate ΔF/F responses.

546 **Locomotion onsets and visual flow onsets.** Locomotion onsets were defined as the locomotion speed
547 crossing a threshold of 0.4 cm/s, where the average speed in the previous two seconds was < 0.4 cm/s,
548 and where the average speed in the subsequent 1 s exceeded 2 cm/s. The same criteria were used to
549 determine visual flow onsets during open loop replays, using the visual flow speed.

550 **LC axonal responses.** For each visual stimulus trigger, the average ΔF/F in the 1 s window prior to stimulus
551 onset was subtracted from the response, before averaging across trials to get the average response of
552 each axon segment. Mismatch and playback halt responses were calculated for each FoV in the 1 s window
553 beginning 0.66 s (40 frames) after stimulus onset. For visual flow onsets during open loop replays, the
554 window was delayed by 400 ms (25 frames) to take into account the slower onset of the stimulus
555 compared to mismatches. Trials were classified as occurring during locomotion if the locomotion speed
556 in the 1 s after the onset of visual flow or mismatch exceeded 1 cm/s, while they were classified as
557 occurring during stationary periods if the locomotion speed was below 1 cm/s. For **Figure 1H**, fast
558 locomotion during mismatch was classified as locomotion speed exceeding 10 cm/s, while slow
559 locomotion was classified as locomotion speed between 1 cm/s and 10 cm/s. For locomotion onset
560 responses (**Figure S2**), the average ΔF/F in the 500 ms window 2 s prior to locomotion onset was
561 subtracted from the response, before averaging across trials. Locomotion onsets were considered to take
562 place during the absence of visual flow if average visual flow speed in the 2 s window centered on
563 locomotion onset was below that corresponding to a 1 cm/s locomotion speed in closed loop conditions.
564 If visual flow speed exceeded this value, the trial was considered to take place during visual flow.
565 Responses for all stimuli were averaged for each FoV across trials only if there were at least three valid
566 trials. For all stimulus conditions that were selected based on locomotion speed (e.g., mismatches), 120

567 sham triggers were generated and sham responses calculated from triggers that were sub-selected based
568 on the same locomotion selection criteria. The average sham response was subtracted from the stimulus
569 response.

570 **V1 layer 2/3 neuron stimulus responses.** For each stimulus trigger, the average ΔF/F in the 1 s window
571 prior to stimulus onset was subtracted from the response, before averaging across trials to get the average
572 response of the neuron. Visual flow and mismatch responses were calculated for each neuron in the
573 window 0.33 s to 2.33 s (5 to 30 frames) after stimulus onset. Trials were classified as occurring during
574 locomotion if the locomotion speed in the 1 s during visual flow or mismatch exceeded 4 cm/s, while they
575 were classified as during stationary periods if the locomotion speed was below 1 cm/s. For mismatches,
576 only locomotion trials were included. Note that for **Figure 3**, visual responses were not segregated into
577 locomotion and stationary trials: all trials were included. For analysis of locomotion modulation index in
578 different locomotion speed conditions (**Figure 5D-G**), slow, medium, and fast locomotion speed trials
579 were categorized where average locomotion speed during visual flow was between 1 and 5 cm/s, 5 and
580 10 cm/s, and above 10 cm/s respectively. For the previously published datasets (**Figure 5**, CT, NR, and NT)
581 (Attinger et al., 2017; Vasilevskaya et al., 2022; Widmer et al., 2022), differences in the measurement of
582 locomotion speed across the datasets made it difficult to use a common threshold value. Thus, to make
583 the locomotion modulation indices comparable to those calculated from the newly acquired dataset
584 (**Figure 5D-G**), we used the 95th percentile of the locomotion speed to normalize thresholds across
585 datasets. In addition, since the visual responses used to measure locomotion modulation index were
586 visual flow onsets in open loop conditions rather than rapid onset fixed speed stimuli, the analysis window
587 relative to stimulus onset was shifted by 400 ms to account for the slower onset. Responses were
588 averaged for each neuron across trials only if there were at least three valid trials. For all stimulus
589 conditions that were selected based on locomotion speed (e.g., mismatches), the average response to
590 1000 sham triggers sub-selected based on the same locomotion conditions was calculated. This sham
591 response was subtracted from the stimulus response.

592 **Locomotion modulation index.** To quantify the change in mean visual flow response during locomotion
593 for each neuron normalized by the overall size of response, we calculated a locomotion modulation index
594 (LMI) for each neuron as follows:

595 $$LMI = \frac{R_{VFloco} - R_{VFstat}}{\sqrt{{R_{VFloco}}^2 + {R_{VFstat}}^2}}$$

596 Where R_{VFloco} is the average visual flow response during locomotion, and R_{VFstat} is the average visual flow
597 response during stationary periods.

598 **Exclusion criteria in analysis of visual plasticity (Figure 4).** Imaging sessions during which the mouse spent
599 less than 15% of the time locomoting at a speed exceeding 4 cm/s were excluded (13 of 71 sessions), as
600 this would limit both the amount of visuomotor coupling experienced during the plasticity assay, and our
601 ability to analyze visual responses during locomotion.

602 **Layer 2/3 functional cell type classification (Figure S3).** Neurons were grouped into visually suppressed
603 and mismatch activated NPE neurons, visually activated PPE neurons, and an intermediate group ('other').
604 Since we were analyzing the visual and mismatch responses of these groups, we used locomotion onset
605 responses to group neurons to avoid a circular analysis. To compute each neuron's locomotion onset
606 response, for each onset the average ΔF/F in the 1 s window beginning 2 s prior to locomotion onset was
607 subtracted from the response, before averaging across trials. Average responses to locomotion onsets
608 (quantified in the window 0.66 to 4 s (10 to 60 frames) after onset) in open loop conditions were
609 subtracted from locomotion onset responses in closed loop conditions (where visual flow is concurrent
610 with locomotion) for each neuron. Note that for analyzing the dataset in **Figure 4**, only the open loop
611 locomotion onsets before LC axon stimulation were used. It was previously shown that the difference
612 between locomotion onset responses in open and closed loop conditions correlates with these cell groups
613 (Jordan and Keller, 2020). For each dataset, the 33rd and 66th percentile of these values were used as
614 thresholds. Neurons with response differences exceeding the 66th percentile were classified as PPE
615 neurons, and those with response differences below the 33rd percentile were classified as NPE neurons,
616 with the remaining neurons were classified as 'other'. Responses to mismatch and visual flow stimuli were
617 consistent with these groupings in all three datasets (**Figure S3**).

618 **Axon density.** PFA fixed brains of mice injected with a vector to express ChrimsonR-tdTomato in NET-
619 positive neurons of the LC were sliced at 40 µm and after mounting, examined under a confocal
620 microscope at 20x magnification. For all mice, images were taken from four sites in V1, each one from a
621 different cortical slice, with sites chosen based on somatic labelling in the green channel (indicating
622 GCaMP expression and a likely two-photon imaging site). To quantify LC axon density, the red channel

623 images were then analyzed. tdTomato labelled axonal segments were manually traced in ImageJ using the
624 NeuronJ plugin (Meijering et al., 2004). The total combined length of the axon segments was then divided
625 by the total area of the cortex in the image to calculate axon density in each image. The average density
626 across four images was taken as the axon density for each mouse. This value was used to distinguish high
627 expression and low expression mice based on a threshold of 0.002 µm per μm^2 (total axon length per unit
628 area of the cortex) (**Figures 4B and S4A**). Since only two mice were categorized to have low expression in
629 the dataset used in **Figure 3**, low expression mice were not included as a separate group in these analyses,
630 and instead excluded.

631 **Statistical tests.** All statistical information for the tests performed in this manuscript are provided in **Table**
632 **S1**. For data where the experimental unit was neurons, we used hierarchical bootstrapping (Saravanan et
633 al., 2020) for statistical testing due to the nested structure (neurons and mice) of the data. To do this, we
634 first resampled the data (with replacement) at the level of imaging sites. From the selected set of imaging
635 sites, we then resampled the data (with replacement) at the level of neurons. We then computed the
636 mean of this bootstrap sample. This would be repeated 10 000 times to generate a distribution of mean
637 values. For paired tests, the p-value was calculated as the proportion of this distribution that was higher
638 or lower than zero, depending on the null hypothesis. For unpaired tests, the p-value was calculated as
639 the proportion of the distribution higher or lower than the values from the distribution of the compared
640 dataset, depending on the hypothesis. For data where the experimental unit was FoV (**Figures 1 and 2**) or
641 mice (pupil dilation, **Figure S4B**), t-tests were used instead, after confirming that the datasets conformed
642 with normality. Datasets that did not conform with normality were compared with Rank-sum tests. Paired
643 data was always tested with paired t-tests (**Figure 1**).

644

MAIN FIGURES

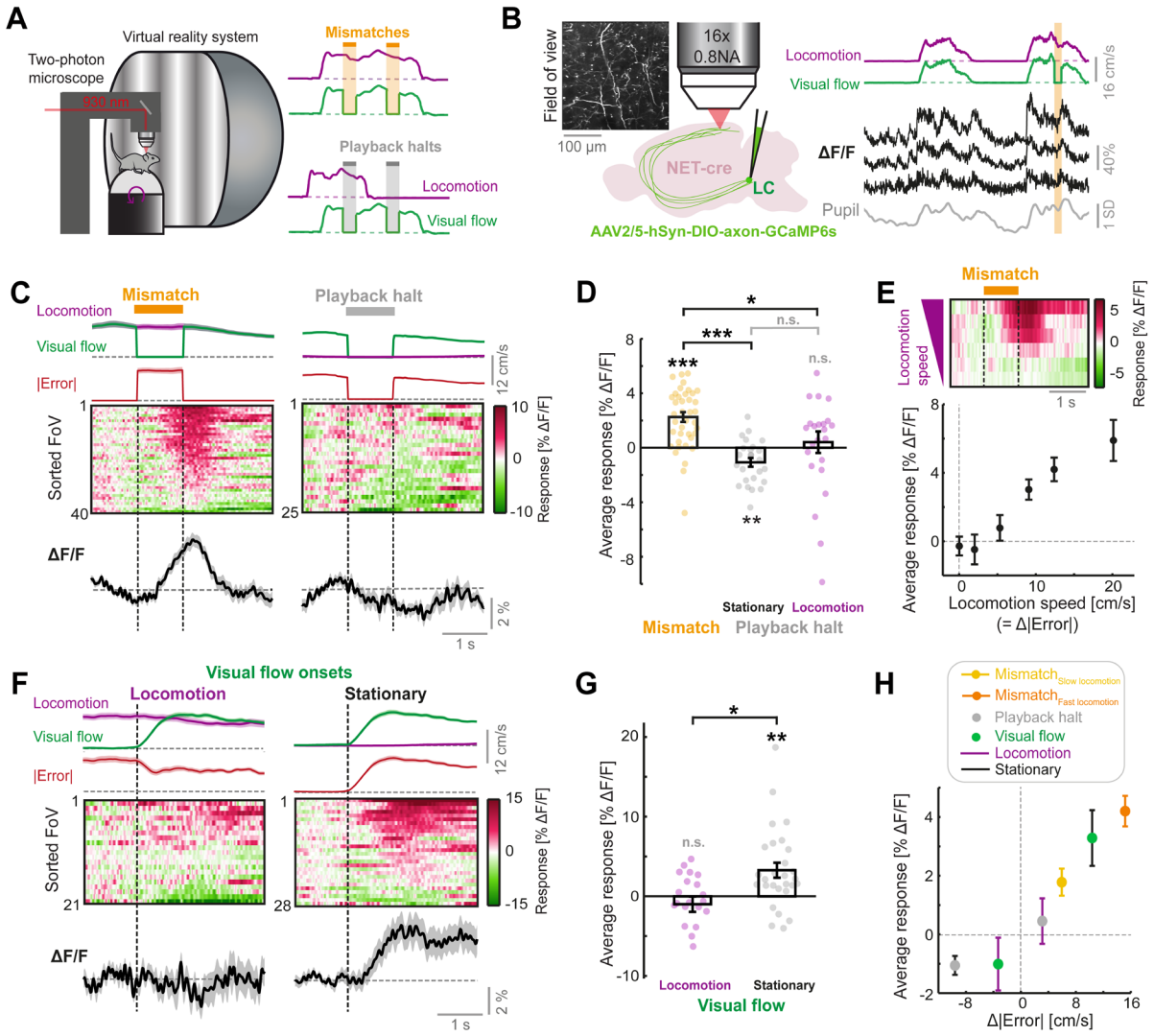

Figure 1. LC axonal calcium activity reflects unsigned visuomotor prediction errors.

(**A**) Left: Schematic of the two-photon microscope and virtual reality system. Right: Schematics of the two virtual reality conditions. Top: closed loop condition in which visual flow speed (green) is yoked to locomotion speed (purple). Mismatches consist of 1 s halts in visual flow during locomotion (orange shading). Bottom: open loop condition in which visual flow from the closed loop session is replayed to the mouse uncoupled from locomotion. Playback halts are 1 s halts in visual flow in the open loop condition (gray shading).

(**B**) Two-photon calcium imaging of LC axons in the dorsal cortex. Left: NET-Cre mice underwent stereotactic viral vector injections to express axon-targeted GCaMP6s in the LC. 4 weeks later, axons were imaged in two regions of the cortex. Inset shows example two-photon field of view (FoV). Right: Example

ΔF/F traces (black) from three different axons segments in the same FoV, recorded during the closed loop condition. Purple and green traces show locomotion and visual flow speed respectively. Orange shading indicates mismatch events. Gray trace shows pupil diameter.

(**C**) Responses of LC axons to visual flow halt stimuli (left: mismatches, and right: playback halts while the mouse is stationary). Top: Locomotion speed (purple), visual flow speed (green) and absolute error (red; absolute difference between visual flow speed and locomotion speed) each averaged across trials. Middle: Heat map of the average responses of different fields of view (FoVs) sorted according to response magnitude. Bottom: Response averaged across FoVs. Shading indicates SEM.

(**D**) Average responses per FoV to mismatches and playback halts, while the mouse was either stationary or locomoting. Error bars indicate SEM across FoVs. Here and in other panels, n.s.: not significant, *: $p < 0.05$, **: $p < 0.01$, ***: $p < 0.001$. For complete statistical information see **Table S1**.

(**E**) Mean mismatch response of LC axons averaged across FoVs as a function of locomotion speed. Top: Heat map of the average mismatch response, sorted according to locomotion speed (speeds correspond to below plot). Bottom: Mean and SEM (error bars) of the mismatch responses averaged over FoVs as a function of locomotion speed. Only datapoints with at least 10 FoVs in each speed bin are included.

(**F**) Responses of LC axons to visual flow onsets in the open loop condition during locomotion (left) or stationary periods (right), plotted as in panel **C**.

(**G**) Average responses of LC axons to visual flow onsets while the mouse was either locomoting or stationary, plotted as in panel **D**.

(**H**) Responses of LC axons to the different visual flow stimuli in different conditions averaged across FoVs, color coded according to the legend, and plotted as a function of the change in absolute error between locomotion speed and visual flow speed during the stimulus (relative to 1 s prior to stimulus onset). Error bars indicate SEM.

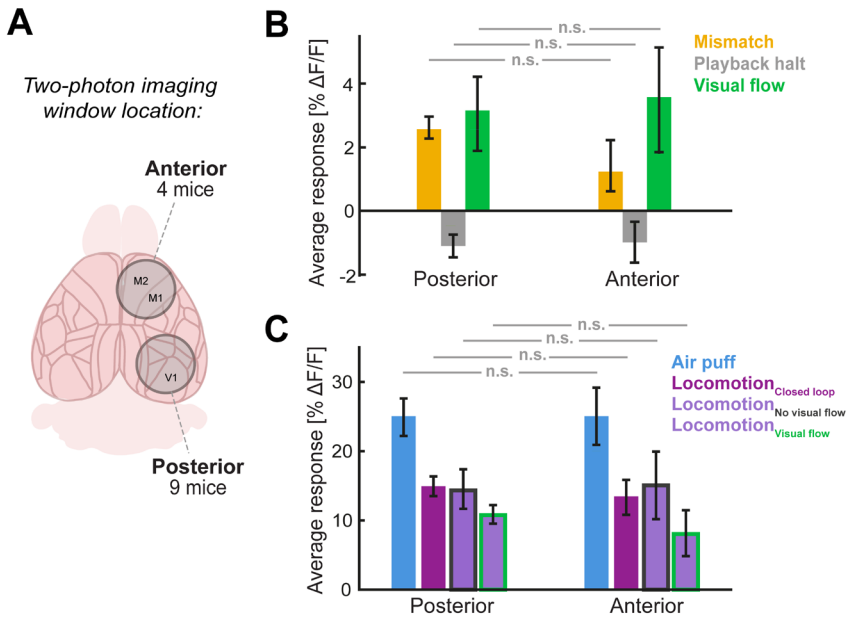

Figure 2. LC axonal responses are indistinguishable in sensory (posterior) and motor (anterior) cortical areas.

(**A**) Schematic of the two different locations of the two-photon imaging windows used. Posterior windows were centered on V1 and included surrounding structures, while anterior windows included the primary and secondary motor cortex.

(**B**) Responses of LC axons to mismatch, playback halt, and visual flow onset averaged across FoVs, compared between posterior and anterior imaging locations. Error bars indicate SEM. Here and in other panels, n.s.: not significant. For complete statistical information see **Table S1**.

(**C**) As in **B**, but for air puff responses (which were infrequently used to evoke locomotion) and locomotion onset responses in various conditions, each averaged in the 3 s window after onset. Note that locomotion$_{\text{Visual flow}}$ and locomotion$_{\text{No visual flow}}$ occur in open loop conditions (see also **Figure S2**).

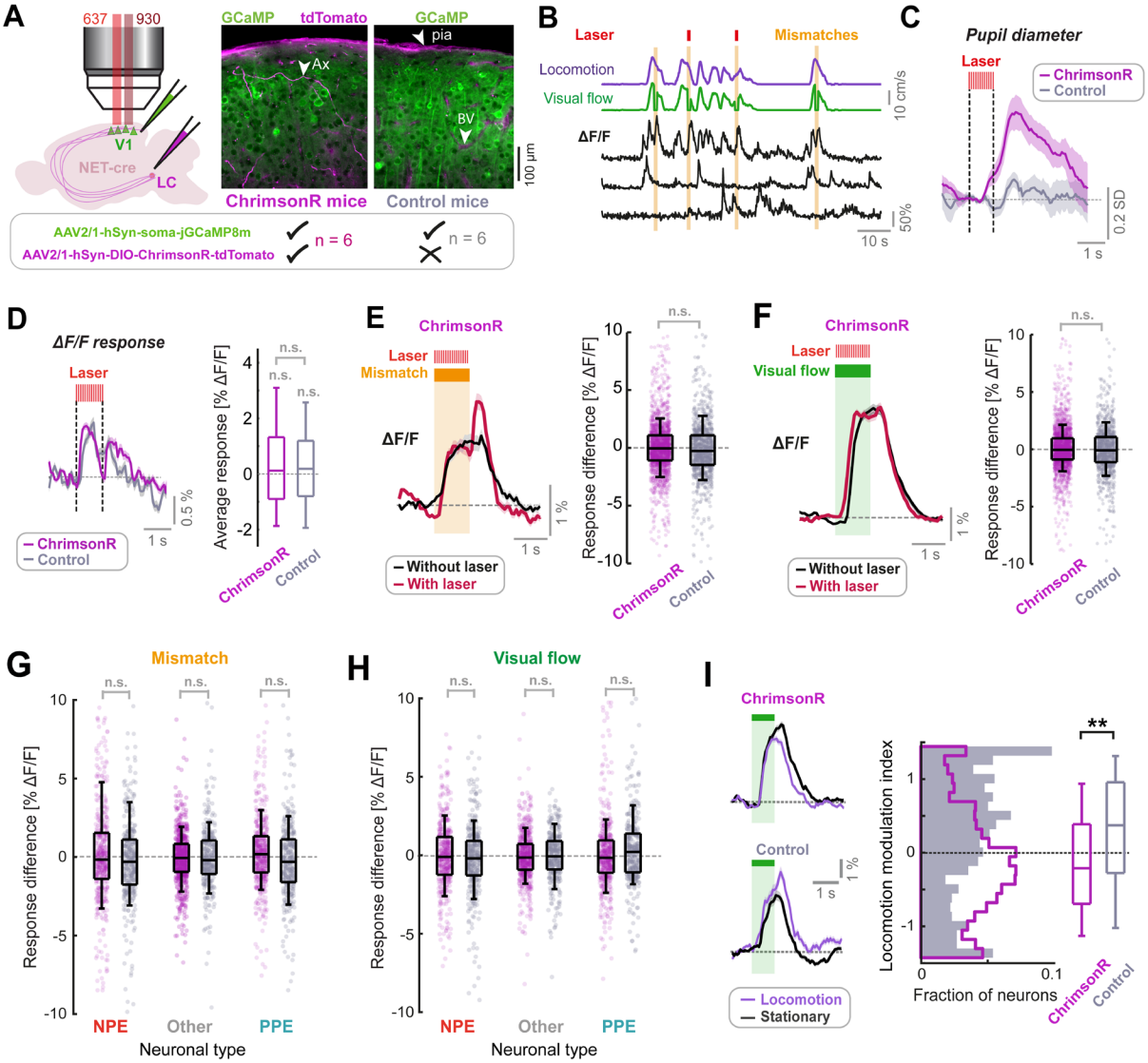

Figure 3. LC axon stimulation has no measurable effect on stimulus responses in layer 2/3 of V1.

(**A**) AAV vector injections were used to express ChrimsonR-tdTomato in LC NET-positive neurons, and jGCaMP8m in layer 2/3 neurons of V1. Simultaneous two-photon calcium imaging and optogenetic stimulation with a 637 nm laser would take place in layer 2/3. Injections into the LC were omitted in control mice. Example histology images indicate expression of jGCaMP8m (green) and tdTomato (magenta); note that blood vessels and pia mater (see arrows labelled 'BV' and 'pia' respectively) are also visible in the magenta channel. Arrow labelled 'Ax' indicates an axon.

(**B**) Example ΔF/F traces for three somatic ROIs in layer 2/3 of V1 (black) and the corresponding visual flow speed (green) and locomotion speed (purple) traces. Orange shading indicates visuomotor mismatch events. Red marks indicate concurrent laser stimulation to activate ChrimsonR on a random subset of mismatch trials.

704 (**C**) Average pupil diameter response to stimulation with the optogenetic laser presented in isolation for
705 ChrimsonR-expressing mice (pink), and control mice (gray). Shading represents SEM.

706 (**D**) Left: Average population ΔF/F response of layer 2/3 neurons in V1 to the onset of the optogenetic
707 stimulation laser presented in isolation. Right: Boxplots to compare average response (quantified in the
708 window 0.3 to 1.6 s after optogenetic stimulation onset) for the two groups of mice. Here and in other
709 panels, n.s.: not significant. For complete statistical information see **Table S1**.

710 (**E**) Analysis of mismatch responses of all layer 2/3 neurons. Left: Average population ΔF/F response of
711 layer 2/3 neurons in V1 of ChrimsonR-expressing mice to visuomotor mismatch either with (red) or
712 without (black) concurrent optogenetic laser stimulation. Right: Boxplots to compare the difference in
713 average mismatch response between trials with and without optogenetic laser stimulation. Pink points
714 indicate data for each neuron from ChrimsonR-expressing mice, and gray points indicate data from control
715 mice. Note, statistical tests against zero for the effect in ChrimsonR-expressing mice were also insignificant
716 (see **Table S1**).

717 (**F**) As for **E**, but for responses to 1 s fixed speed visual flow stimuli in open loop conditions.

718 (**G**) As for boxplots in panel **E**, but for mismatch responses of three different functionally defined neuronal
719 groups: NPE = negative prediction error neurons, with large responses to mismatches, PPE = positive
720 prediction error neurons, with large responses to visual flow, and an intermediate group 'other'. See
721 Methods and **Figure S3** for information on neuronal types. Note, statistical tests against zero for the effect
722 in ChrimsonR-expressing mice were also insignificant (see **Table S1**).

723 (**H**) As for **G**, but for responses to 1 s fixed speed visual flow stimuli in open loop conditions.

724 (**I**) Left: Population average responses to visual flow stimuli during stationary periods (black) and during
725 locomotion (purple), for control mice (bottom), and ChrimsonR-expressing mice (top). Shading represents
726 SEM. Note that only trials *without* concurrent optogenetic stimulation are included here. Right:
727 Histograms and boxplots to show distribution of locomotion modulation index for the visual responses
728 recorded in control (gray) and ChrimsonR-expressing mice (pink). Here, **: $p < 0.01$ (see **Table S1**).

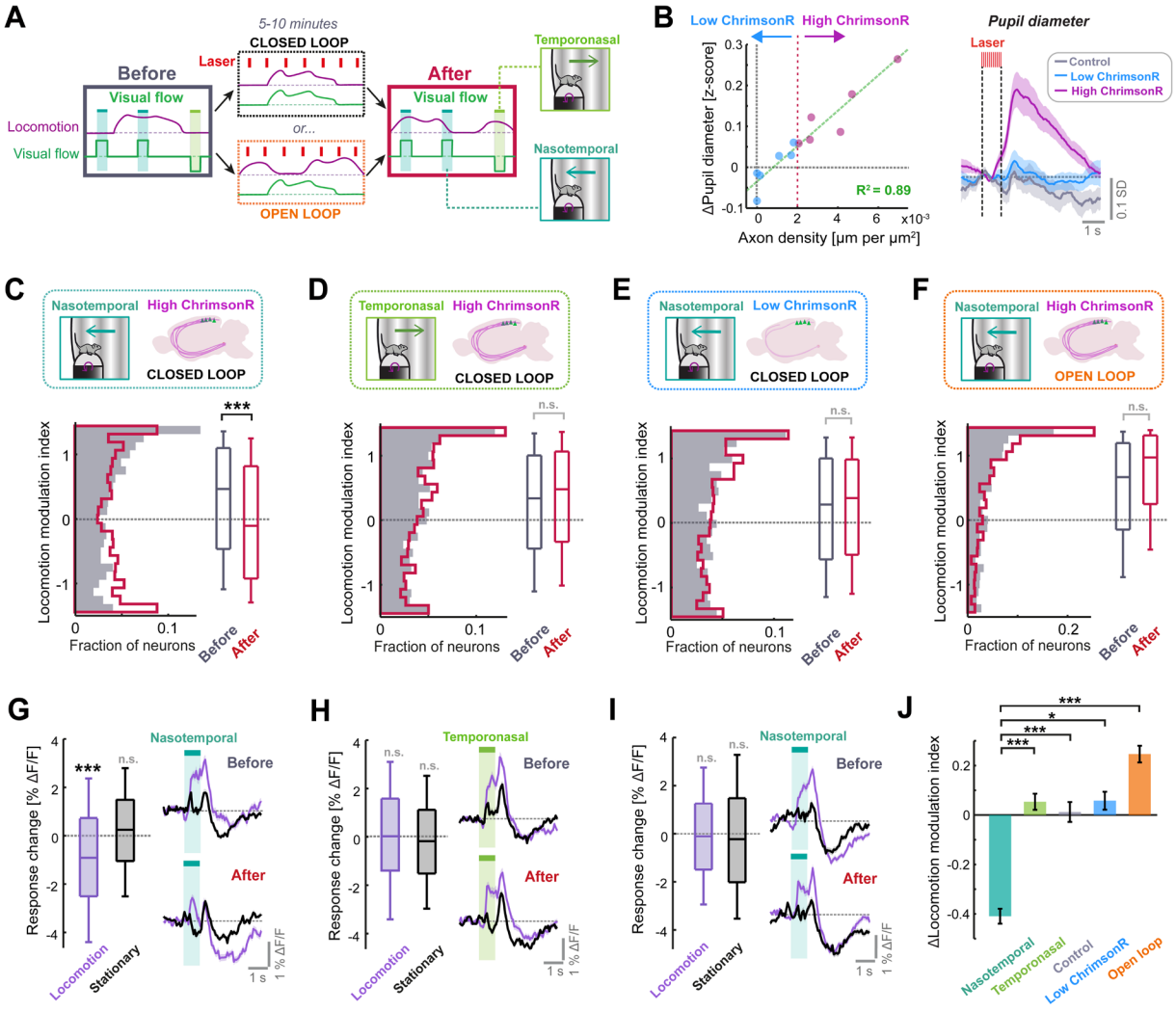

Figure 4. Phasic LC output enhances sensorimotor plasticity in layer 2/3 of V1.

(**A**) Diagram of the experiment used to determine whether LC axon stimulation during different visuomotor coupling conditions can modulate plasticity. Visual responses are compared before and after 5-10 minutes of either closed or open loop conditions, during which LC axons were stimulated every 7 s on average.

(**B**) Left: Scatter plot to show the relationship between density of ChrimsonR-tdTomato labelled axons in V1 (total axon length per unit area of the cortex, analyzed postmortem) and the average evoked pupil dilation during optogenetic stimulation. Green dashed line is a linear regression fit to the data, and red dotted line indicates axon density threshold used to categorize low (blue) and high (pink) ChrimsonR-expressing mice. Right: Average pupil diameter response to stimulation with the optogenetic laser for 6 mice with high ChrimsonR expression in LC axons (pink), 6 mice with low ChrimsonR expression (blue), and 7 control mice that did not receive a vector injection into the LC (black). Shading represents SEM over sessions.

743 (**C**) Analysis of plasticity in nasotemporal visual flow responses in ChrimsonR-expressing mice undergoing
744 optogenetic laser stimulation during closed loop visuomotor experience. Histograms and boxplots show
745 distribution of locomotion modulation indices for the visual responses of layer 2/3 V1 neurons recorded
746 before (dark gray) and after the stimulation period (red). Here and in all other panels: n.s.: not significant,
747 *: $p < 0.05$, **: $p < 0.01$, ***: $p < 0.001$. See **Table S1** for all statistical information.

748 (**D**) As for panel **C**, but for temporonasal visual flow responses.

749 (**E**) As for panel **C**, but for low ChrimsonR-expressing mice.

750 (**F**) As for panel **C**, but for the condition in which optogenetic stimulation occurred during open loop
751 replays of visual flow (i.e., no visuomotor coupling).

752 (**G**) Analysis of plasticity in nasotemporal visual flow responses in high ChrimsonR-expressing mice
753 undergoing optogenetic laser stimulation during the closed loop condition. Left: Boxplots of the change
754 in response to visual flow after optogenetic stimulation for responses recorded during locomotion
755 (purple) and those recorded during stationary periods (black). Right: Average population response to
756 visual flow during locomotion (purple) and during stationary periods (black), before (top) and after
757 (bottom) optogenetic stimulation. Shading indicates SEM.

758 (**H**) As for panel **G**, but for temporonasal visual flow responses.

759 (**I**) As for panel **G**, but for low ChrimsonR-expressing mice.

760 (**J**) Change in locomotion modulation index after optogenetic stimulation, for the four sets of
761 experiments from panels **C** (nasotemporal), **D** (temporonasal), **Figure S4C** (Control), **E** (low ChrimsonR
762 expression), and **F** (open loop) (presented in the respective sequence).

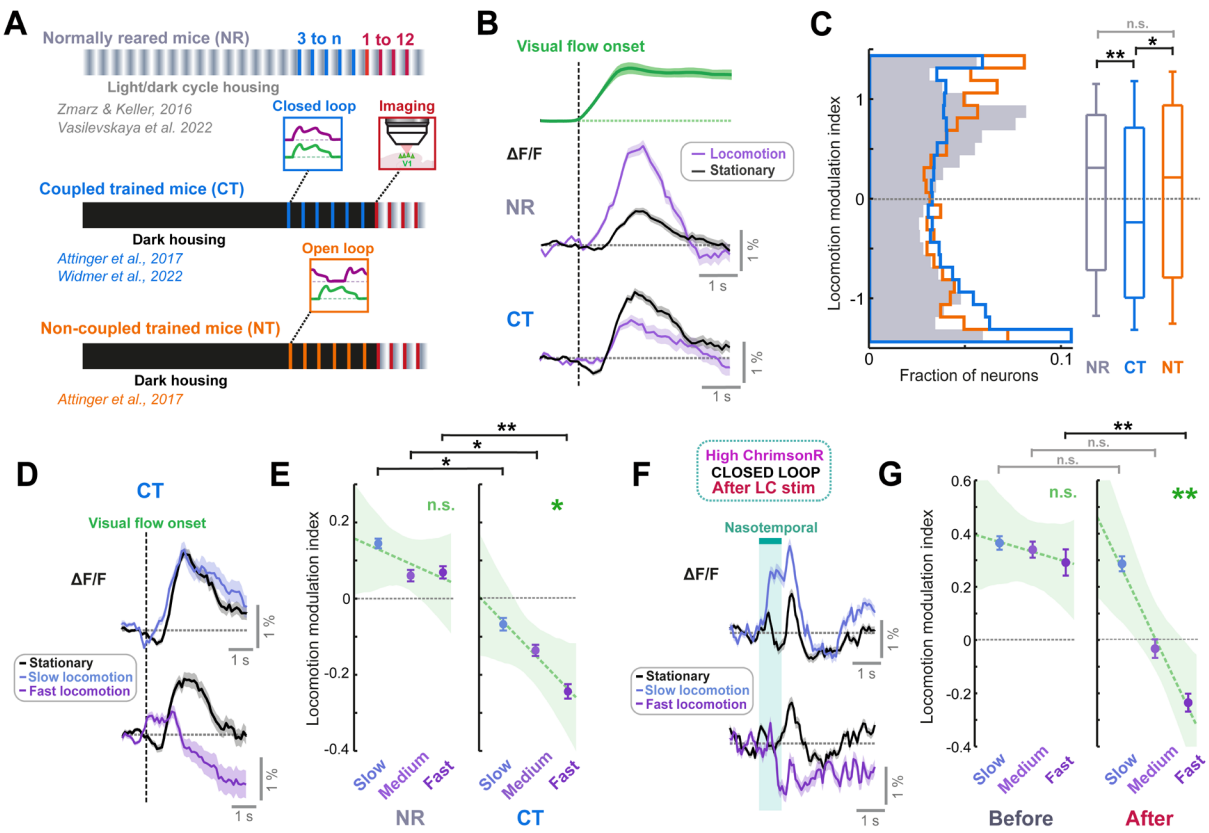

Figure 5. LC axon stimulation over minutes recapitulates the visuomotor plasticity seen over days.

(**A**) Diagram of the three groups of mice reared with different visuomotor experience. Normally reared mice (NR, gray) were raised with a normal light/dark cycle in their cages, with the full diversity of visuomotor coupling in freely moving conditions. Coupled trained mice (CT, blue) were reared in the dark, and their only visuomotor experience prior to imaging was during closed loop conditions in the virtual reality system. Non-coupled trained mice (NT, orange) were reared similar to coupled trained mice, except their only visual experience was during open loop conditions in the virtual reality system.

(**B**) Average population responses of layer 2/3 neurons in V1 to the onset of visual flow during open loop replay sessions. Green shows the average speed profile of the visual flow stimulus, purple shows the average population responses during locomotion, and black shows the average population responses during stationary periods for normally reared (top) and coupled trained (bottom) mice. Shading indicates SEM.

(**C**) Distribution of the locomotion modulation indices of all V1 layer 2/3 neurons for the visual flow onset responses recorded in normally reared (gray), coupled trained (blue), and non-coupled trained (orange) mice. Here and in other panels, n.s.: not significant, *: $p < 0.05$, **: $p < 0.01$, ***: $p < 0.001$. For complete statistical information see **Table S1**.

(**D**) Average population responses of layer 2/3 neurons in V1 in coupled trained mice to the onset of visual flow during stationary periods (black), and during slow (top) and fast (bottom) locomotion (purple). Shading indicates SEM.

783 (**E**) Comparison of locomotion modulation indices averaged across neurons for visual flow onset responses
784 recorded during slow, medium, and fast locomotion speeds, in normally reared (left) and coupled trained
785 (right) mice. Error bars indicate SEM. Green dashed line indicates linear regression fit to the data, and
786 shading indicates the 95% confidence interval of the regression. Green asterisks and 'n.s.' indicate
787 significance of the fit.

788 (**F**) As for panel **D**, but for nasotemporal visual flow responses in high ChrimsonR-expressing mice after LC
789 axon stimulation in closed loop conditions.

790 (**G**) As for panel **E**, but for nasotemporal visual flow responses in high ChrimsonR-expressing mice before
791 (left) and after (right) LC axon stimulation in closed loop visuomotor coupling.

792

SUPPLEMENTARY FIGURES

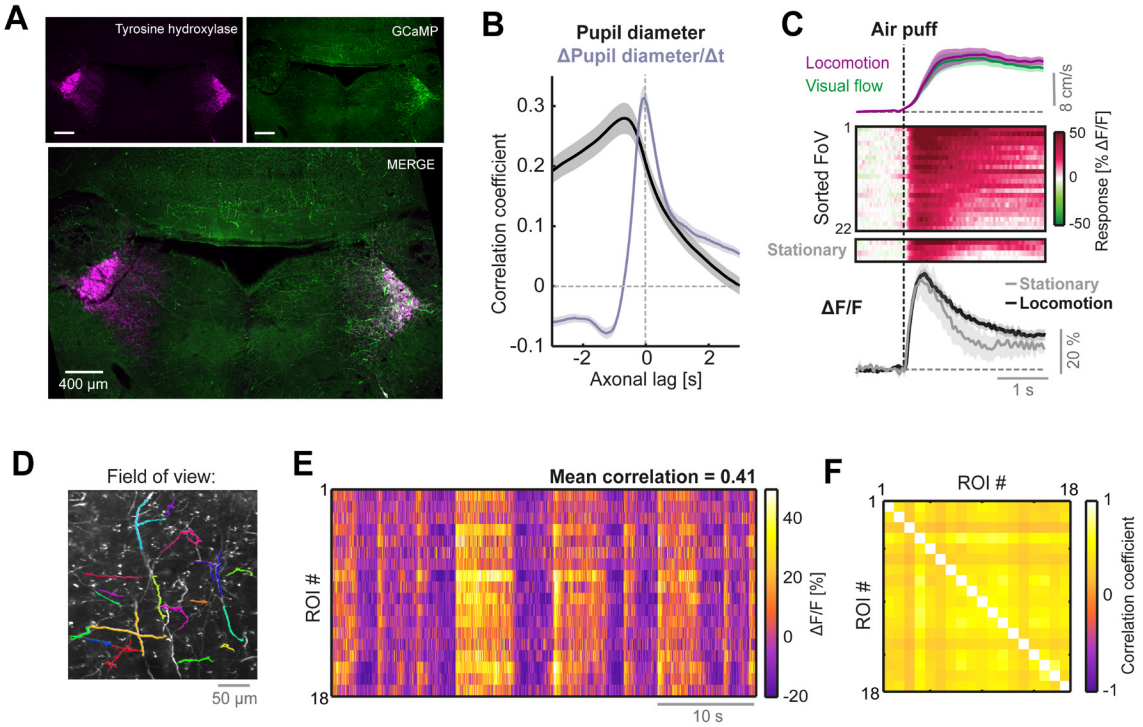

Figure S1. Additional information and analyses on two-photon imaging of LC axons. Related to Figure 1.

(**A**) Confocal micrographs showing immunolabelling for tyrosine hydroxylase (magenta) and GCaMP6s (green) in the two LC. GCaMP6s was expressed via stereotactic viral vector injection into only the right LC of NET-Cre mice.

(**B**) Cross-correlations between LC axonal ΔF/F and pupil diameter (black) or the time derivative of pupil diameter (gray) averaged across 40 FoVs. Shading indicates SEM. Positive axonal lag values indicate time delays where axonal fluorescence lags relative to pupil diameter or its derivative.

(**C**) Responses to air puff stimuli applied to the flank which were infrequently used to evoke locomotion (here during the closed loop condition). Top: Average locomotion speed (purple) and visual flow speed (green) for trials that evoked locomotion. Middle: Heat maps of the average air puff responses of different FoVs sorted according to response magnitude, for trials that evoked locomotion (top heat map) and rare trials that did not evoke locomotion (bottom heat map). Bottom: Response averaged across FoVs for air puff trials that evoked locomotion (black) and those that did not (gray). Shading indicates SEM.

(**D**) Example two-photon field of view of LC axons, with 18 regions of interest (ROI) superimposed in different colors.

(**E**) Heat map of ΔF/F of the 18 ROIs in panel **D** from a segment of closed loop experience.

(**F**) Correlation matrix of the activity of the 18 different ROIs in panels **D** and **E**.

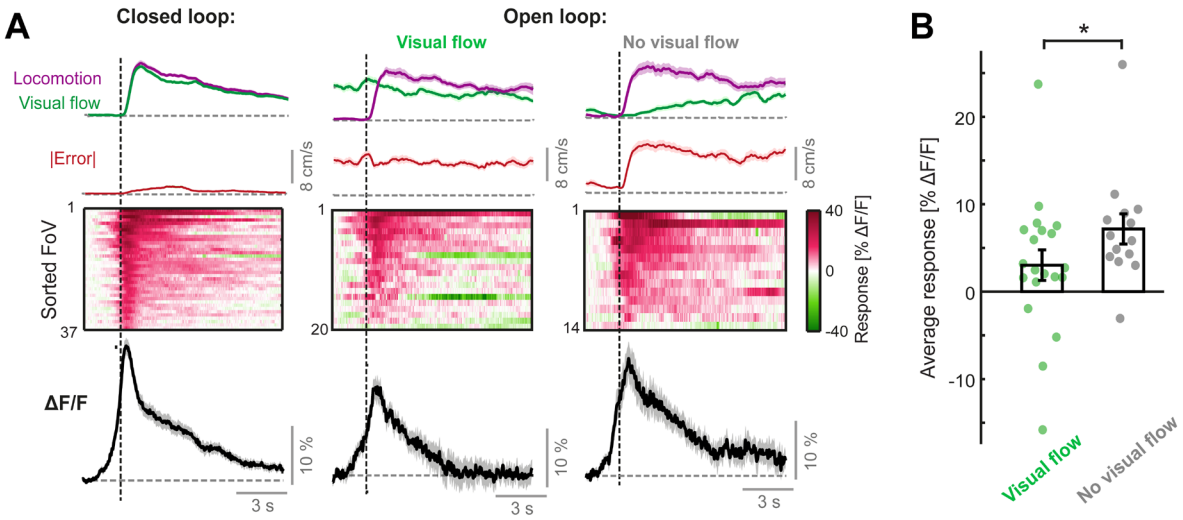

Figure S2. Locomotion onset responses of LC axons. Related to Figure 2.

(**A**) Responses to the onset of locomotion occurring during the closed loop condition (left), during visual flow in the open loop condition (middle), and during no visual flow in the open loop condition (right). Top: Average visual flow speed (green) and locomotion speed (purple) averaged across trials. Note that the window for defining the occurrence of visual flow is in the 2 s window centered on the locomotion onset – therefore the incidence of visual flow increases away from this onset. Red trace shows the absolute error between locomotion speed and visual flow speed averaged across trials (note that, since absolute error is averaged across trials independently, it is *not* equivalent to the absolute difference in averaged locomotion speed and visual flow speed traces plotted above. In addition, note that the minor error occurring in the closed loop condition is due to mismatches). Middle: Heat map of the average responses of different fields of view (FoV) sorted according to response magnitude. Bottom: Response averaged over FoVs. Shading indicates SEM.

(**B**) Comparison of average sustained response of LC axons to locomotion onsets in the open loop condition (quantified in the window 1 to 10 s after locomotion onset), during either visual flow or no visual flow, across FoVs. Each point indicates the average response of an individual FoV. Error bars indicate SEM. *: $p < 0.05$. For statistical information see **Table S1**.

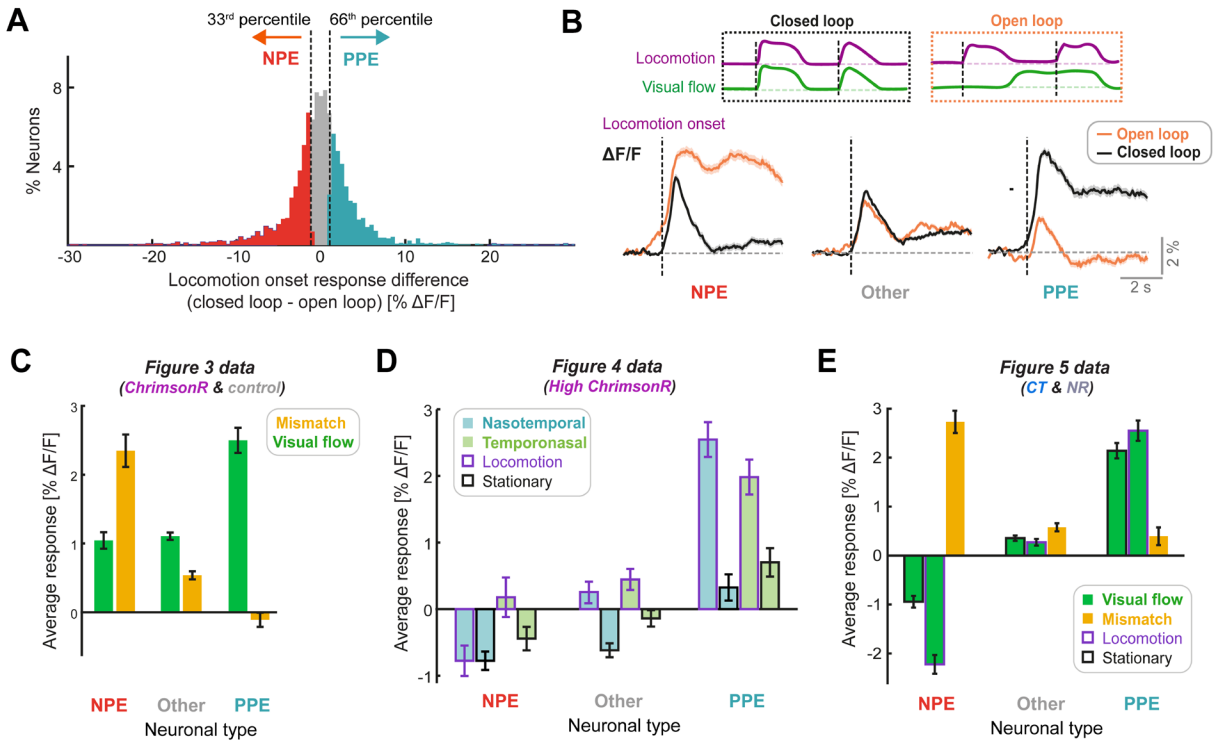

Figure S3. Classification of functional neuronal types in V1 layer 2/3. Related to Figures 3, 4, and 5.

(**A**) Percentage of neurons as a function of the difference in response to locomotion onsets in closed loop conditions and open loop conditions. Neurons with a responses difference below the 33rd percentile (open loop response > closed loop response), were classified as visually suppressed NPE neurons (red), while those with a response difference exceeding the 66th percentile (closed loop response > open loop response), were classified as visually driven PPE neurons (turquoise), as shown. Data for this panel comes from **Figure 3** dataset.

(**B**) Top: Diagram of visual flow and locomotion speed traces to indicate closed loop and open loop locomotion onsets (black dashed lines). Bottom: Responses to locomotion onset during closed loop and open loop, averaged across neurons classified as NPE, PPE, and the intermediate group (Other). Shading indicates SEM. Data for this panel comes from **Figure 3** dataset.

(**C**) Bar graph to show visual flow and visuomotor mismatch responses, averaged across neurons, compared for the three functional neuron types: NPE, Other, and PPE neurons. Error bars indicate SEM. Data for this panel comes from **Figure 3** dataset.

(**D**) Bar graph to show nasotemporal and temporonasal visual flow responses (split further into occurring during locomotion or stationary periods), averaged across neurons, compared for the three functional neuron types: NPE, Other, and PPE neurons. Error bars indicate SEM. Data for this panel comes from **Figure 4** dataset (High ChrimsonR only). Mismatch data was not acquired for this dataset.

(**E**) Bar graph to show visual flow onset and visuomotor mismatch responses, averaged across neurons, compared between NPE, Other, and PPE cell classes. Error bars indicate SEM. Data for this panel comes from **Figure 5** datasets (coupled trained and normally reared mice).

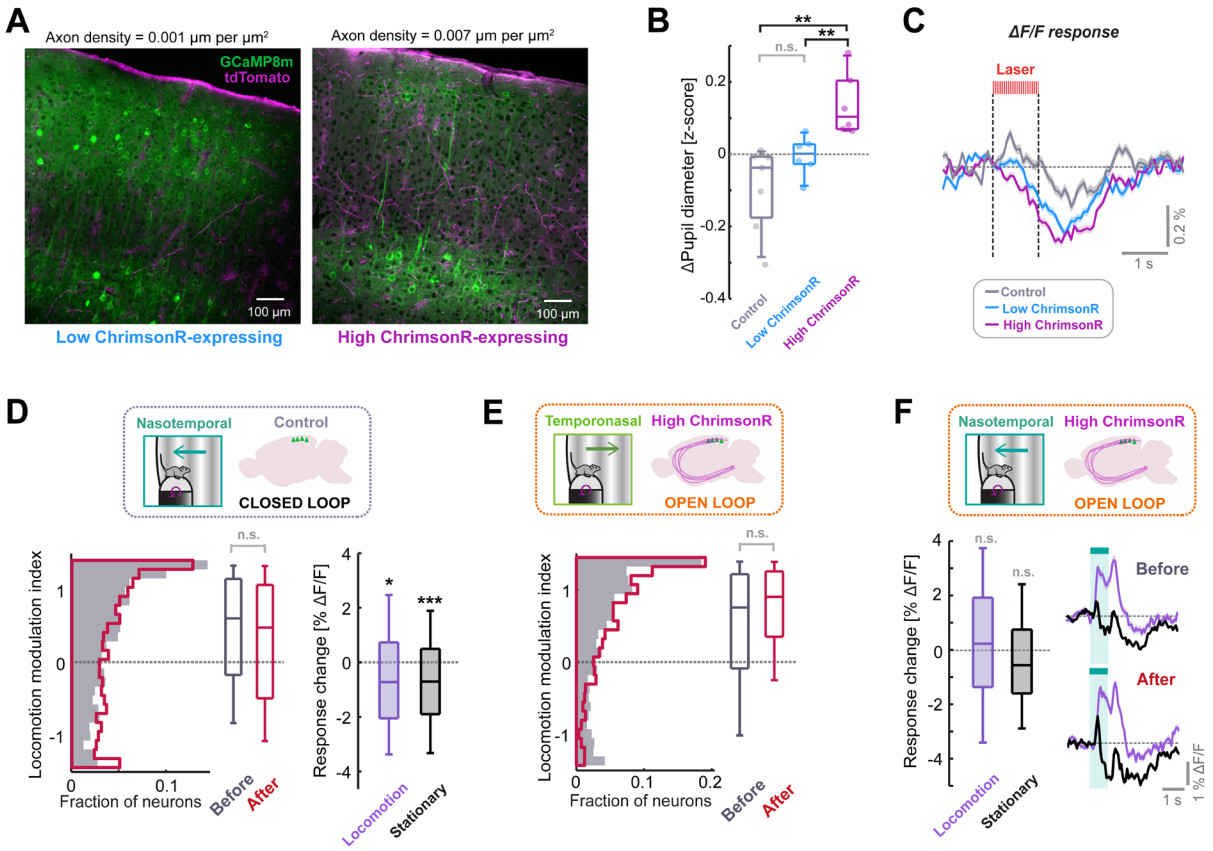

852

853 **Figure S4. Additional information and analyses on optogenetic stimulation of LC axons to drive**
854 **plasticity. Related to Figure 4.**

855 (**A**) Two example confocal microscopy images from V1 showing jGCaMP8m expression (green) and
856 tdTomato expression (magenta), indicating labelled LC axons. The right image is from an animal classified
857 as high ChrimsonR-expressing, based on labelled axon density, and left image is from an animal classified
858 as low ChrimsonR-expressing.

859 (**B**) Comparison of average pupil diameter response (quantified in the window 1.3 to 4.7 s after
860 optogenetic stimulation onset) for control, low ChrimsonR-expressing and high ChrimsonR-expressing
861 mice. Here and in other panels, n.s.: $p > 0.05$, *: $p < 0.05$, **: $p < 0.01$, ***: $p < 0.001$. For complete
862 statistical information see **Table S1**.

863 (**C**) Average population ΔF/F response of layer 2/3 neurons in V1 to the onset of the optogenetic
864 stimulation laser. Shading indicates SEM. Note that optogenetic laser power was lowered compared to
865 the value used in **Figure 3**, and the positive response seen in **Figure 3D** is no longer evident.

866 (**D**) Analysis of plasticity in nasotemporal visual flow responses in control mice which underwent
867 optogenetic laser stimulation during the closed loop condition. Left: Distribution of locomotion
868 modulation index for the visual responses recorded before (dark gray) and after the stimulation period
869 (red). Right: Change in ΔF/F response to visual flow after optogenetic stimulation for responses recorded
870 during locomotion (purple) and during stationary periods (black).

871 (**E**) As for panel **D**, but for temporonasal visual flow responses recorded in high ChrimsonR-expressing
872 mice, where optogenetic stimulation occurred during open loop replays of visual flow (i.e., uncoupled
873 from locomotion).

874 (**F**) Analysis of plasticity in nasotemporal visual flow responses for high ChrimsonR-expressing mice which
875 underwent optogenetic laser stimulation during open loop replays of visual flow (i.e., uncoupled from
876 locomotion). Boxplot shows the change in ΔF/F response to visual flow after optogenetic stimulation for
877 responses recorded during locomotion (purple) and during stationary periods (black). Traces show
878 average population response to visual flow during locomotion (purple) and during stationary periods
879 (black), before (top) and after (below) optogenetic stimulation. Shading indicates SEM.

880

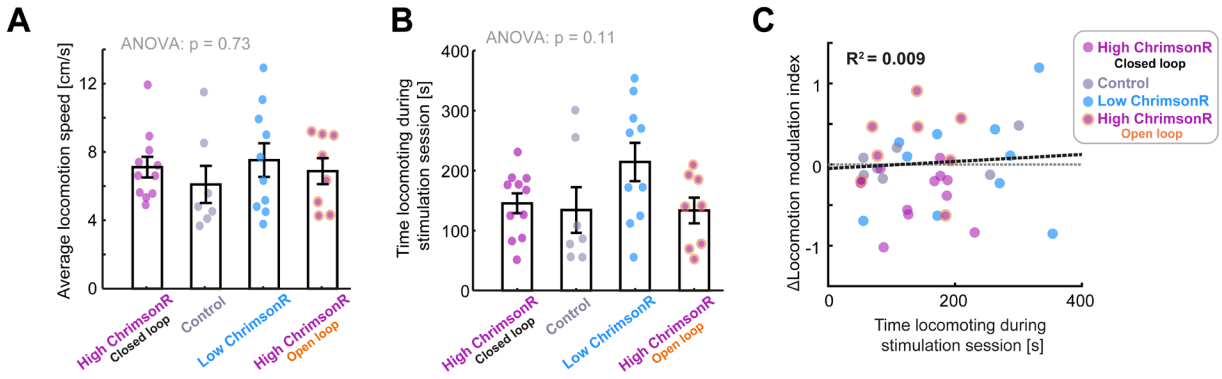

Figure S5. Differences in locomotion during stimulation cannot explain differences in the change of locomotion modulation index between groups. Related to Figure 4.

(**A**) Average locomotion speed (excluding stationary periods) for: High ChrimsonR-expressing mice during closed loop stimulation, Control mice during closed loop stimulation, low ChrimsonR-expressing mice during closed loop stimulation, and high ChrimsonR-expressing mice during open loop stimulation. Points show data for each imaging session.

(**B**) As for panel **A**, but for the time spent engaged in locomotion during the stimulation period.

(**C**) Change in locomotion modulation index after optogenetic stimulation plotted against the time spent engaged in locomotion during the laser stimulation period of the imaging session. Each point shows the averages for a single imaging session.

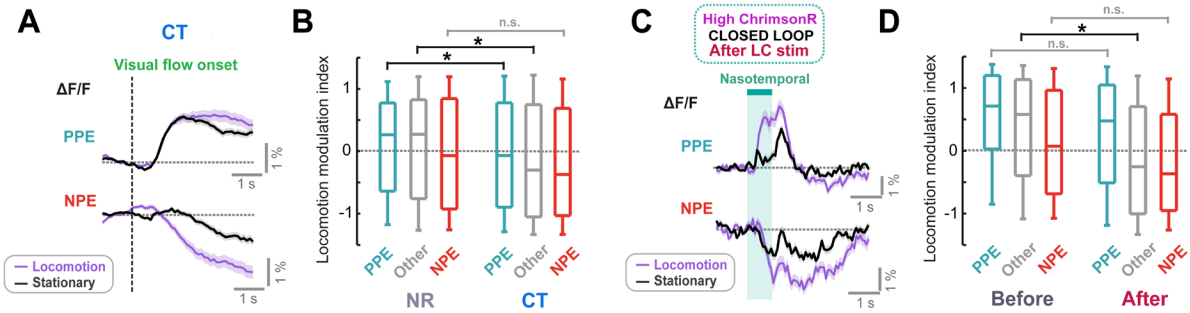

Figure S6. Comparison of locomotion modulation index across different functional neuronal types in layer 2/3 V1. Related to Figure 5.

(**A**) Average population responses of layer 2/3 neurons in V1 in coupled trained mice to the onset of visual flow during stationary periods (black), and during locomotion (purple) for visually driven positive prediction error neurons (PPE, top) and visually suppressed negative prediction error neurons (NPE, bottom). Shading indicates SEM.

(**B**) Comparison of locomotion modulation index for visual flow onset responses of positive (turquoise), negative (orange) prediction error neurons, and an intermediate population of neurons (gray), recorded in normally reared (left) and coupled trained (right) mice. For information on functional neuron types, see **Figure S3**. Here and in other panels, n.s.: $p > 0.05$, *: $p < 0.05$, **: $p < 0.01$, ***: $p < 0.001$. For complete statistical information see **Table S1**.

(**C**) As for panel **A**, but for nasotemporal visual flow responses in high ChrimsonR-expressing mice after LC axon stimulation in closed loop conditions.

(**D**) As for panel **B**, but for nasotemporal visual flow responses in high ChrimsonR-expressing mice before (left) and after (right) LC axon stimulation in closed loop conditions.

TABLES

Table S1. All statistical information.

Figure panel	Comparison	Value compared	Mean 1 *(delta shown for paired tests)*	SD 1	Mean 2 *(n/a for paired tests)*	SD 2	Test type	P-value	N (ROIs)	N (Sites)	N (Mice)
1D	Mean response *vs* zero	Playback halt response (stationary) [% ΔF/F]	-1.07	1.61	n/a	n/a	Unpaired t-test	**0.0028**	n/a	25	10
	Mismatch *vs* Playback halt (locomotion)	Mean response [% ΔF/F]	2.26	2.30	0.41	3.86	Unpaired t-test	**0.0189**	n/a	40,24	10,13
	Playback halt locomotion *vs* stationary	Mean response [% ΔF/F]	0.41	3.86	-1.07	1.61	Unpaired t-test	0.0849	n/a	24,25	10,10
	Mean response *vs* zero	Playback halt response (locomotion) [% ΔF/F]	0.41	3.86	n/a	n/a	Unpaired t-test	0.6113	n/a	24	10
	Mean response *vs* zero	Mismatch response [% ΔF/F]	2.26	2.30	n/a	n/a	Unpaired t-test	**$< 10^{-5}$**	n/a	40	13
	Mismatch *vs* Playback halt (stationary)	Mean response [% ΔF/F]	2.26	2.30	-1.07	1.61	Unpaired t-test	**$< 10^{-5}$**	n/a	40,25	10,13
1G	Mean response *vs* zero	Visual flow response (stationary) [% ΔF/F]	3.27	5.01	n/a	n/a	Unpaired t-test	**0.0027**	n/a	28	11
	Locomotion *vs* stationary	Mean visual response [% ΔF/F]	-1.00	4.41	3.27	5.01	Rank-sum	**0.0070**	n/a	21,28	11,11
	Mean response *vs* zero	Visual flow response (locomoting) [% ΔF/F]	-1.00	4.41	n/a	n/a	Unpaired t-test	0.4853	n/a	21	11
2B	Posterior *vs* Anterior	Mismatch response [% ΔF/F]	2.57	2.02	1.18	2.95	Unpaired t-test	0.1115	n/a	31, 9	9,4
	Posterior *vs* Anterior	Playback halt response (stationary) [% ΔF/F]	-1.12	1.43	-0.98	1.98	Unpaired T-test	0.8401	n/a	16, 9	6, 4
	Posterior *vs* Anterior	Visual flow response (stationary) [% ΔF/F]	3.14	5.13	3.55	5.02	Unpaired T-test	0.8426	n/a	19, 9	7, 4
2C	Posterior *vs* Anterior	Locomotion response (visual flow) [% ΔF/F]	10.85	5.89	8.12	8.46	Unpaired T-test	0.4146	n/a	14, 6	6, 3
	Posterior *vs* Anterior	Locomotion response (closed loop) [% ΔF/F]	14.99	7.07	13.33	7.86	Unpaired T-test	0.5535	n/a	28, 9	9,4
	Posterior *vs* Anterior	Locomotion response (no visual flow) [% ΔF/F]	14.42	8.05	14.96	11.93	Unpaired T-test	0.9202	n/a	8, 6	6, 3
	Posterior *vs* Anterior	Air puff response [% ΔF/F]	24.73	10.03	24.85	11.58	Unpaired T-test	0.9804	n/a	13, 8	6,4
3D	Mean response *vs* zero	ChrimsonR, laser response [% ΔF/F]	0.41	2.68	n/a	n/a	Bootstrap	0.0775	1985	15	6
	Mean response *vs* zero	Control, laser response [% ΔF/F]	0.30	2.24	n/a	n/a	Bootstrap	0.1785	1026	10	6
	Control *vs* ChrimsonR	Laser response [% ΔF/F]	0.30	2.24	0.41	2.68	Bootstrap	0.3929	1026, 1985	10,15	6,6
3E	Control *vs* ChrimsonR	Mismatch response difference [% ΔF/F]	-0.26	3.39	0.05	2.86	Bootstrap	0.2244	1053, 1911	10,14	6,6
	Optogenetic stimulation *vs* no stimulation	ChrimsonR, mismatch response [% ΔF/F]	0.05	2.86	n/a	n/a	Bootstrap	0.4189	1911	14	6
3F	Control *vs* ChrimsonR	Visual flow response difference [% ΔF/F]	-0.04	2.43	0.06	2.34	Bootstrap	0.2296	1053, 2233	10,16	6,6
	Optogenetic stimulation *vs* no stimulation	ChrimsonR, visual flow response [% ΔF/F]	0.06	2.34	n/a	n/a	Bootstrap	0.3869	2233	16	6
3G	Control *vs* ChrimsonR	NPE, mismatch response difference [% ΔF/F]	-0.20	2.97	0.25	2.93	Bootstrap	0.1432	369, 541	10,12	6,6
	Control *vs* ChrimsonR	PPE, mismatch response difference [% ΔF/F]	-0.47	4.41	0.21	3.81	Bootstrap	0.1771	382, 525	10,12	6,6
	Optogenetic stimulation *vs* no stimulation	ChrimsonR NPE, mismatch response [% ΔF/F]	0.25	2.93	n/a	n/a	Bootstrap	0.2177	541	12	6
	Optogenetic stimulation *vs* no stimulation	ChrimsonR PPE, mismatch response [% ΔF/F]	0.21	3.81	n/a	n/a	Bootstrap	0.3433	525	12	6
	Control *vs* ChrimsonR	Other, mismatch response difference [% ΔF/F]	-0.02	2.22	-0.08	1.92	Bootstrap	0.5335	275, 526	10,12	6,6
	Optogenetic stimulation *vs* no stimulation	ChrimsonR Other, mismatch response [% ΔF/F]	-0.08	1.92	n/a	n/a	Bootstrap	0.6313	526	12	6

3H	Control *vs* ChrimsonR	NPE, visual flow response difference [% ΔF/F]	0.33	2.86	0.09	3.19	Bootstrap	0.1432	369, 541	10,12	6,6
	Control *vs* ChrimsonR	PPE, visual flow response difference [% ΔF/F]	-0.20	2.18	-0.19	2.31	Bootstrap	0.1771	382, 525	10,12	6,6
	Optogenetic stimulation *vs* no stimulation	ChrimsonR NPE, visual flow response [% ΔF/F]	0.09	3.19	n/a	n/a	Bootstrap	0.3983	541	12	6
	Control *vs* ChrimsonR	Other, visual flow response difference [% ΔF/F]	-0.13	1.79	-0.08	1.49	Bootstrap	0.5335	275, 526	10,12	6,6
	Optogenetic stimulation *vs* no stimulation	ChrimsonR Other, visual flow response [% ΔF/F]	-0.08	1.49	n/a	n/a	Bootstrap	0.6316	526	12	6
	Optogenetic stimulation *vs* no stimulation	ChrimsonR PPE, visual flow response [% ΔF/F]	-0.19	2.31	n/a	n/a	Bootstrap	0.7564	525	12	6
3I	Control *vs* ChrimsonR	Locomotion modulation index	0.23	0.84	-0.14	0.72	Bootstrap	**0.0012**	816, 1687	8,13	5,6
4C	Before *vs* After	Locomotion modulation index	-0.41	0.99	n/a	n/a	Bootstrap	**< 10^{-5}**	1066	11	5
4D	Before *vs* After	Locomotion modulation index	0.05	1.09	n/a	n/a	Bootstrap	0.7321	1111	11	5
4E	Before *vs* After	Locomotion modulation index	0.06	1.22	n/a	n/a	Bootstrap	0.5922	1140	10	5
4F	Before *vs* After	Locomotion modulation index	0.25	0.97	n/a	n/a	Bootstrap	0.921	832	8	4
4G	Before *vs* After	Visual response (locomotion) [% ΔF/F]	-0.88	3.54	n/a	n/a	Bootstrap	**0.0005**	1066	11	5
	Before *vs* After	Visual response (stationary) [% ΔF/F]	0.17	2.36	n/a	n/a	Bootstrap	0.6929	1276	13	5
4H	Before *vs* After	Visual response (stationary) [% ΔF/F]	-0.17	2.61	n/a	n/a	Bootstrap	0.2579	1276	13	5
	Before *vs* After	Visual response (locomotion) [% ΔF/F]	-0.06	3.34	n/a	n/a	Bootstrap	0.4043	1111	11	5
4I	Before *vs* After	Visual response (stationary) [% ΔF/F]	-0.28	2.97	n/a	n/a	Bootstrap	0.2404	1140	10	5
	Before *vs* After	Visual response (locomotion) [% ΔF/F]	-0.08	2.61	n/a	n/a	Bootstrap	0.3878	1344	12	5
4J	Open loop *vs* Nasotemporal	Δ locomotion modulation index	0.25	0.97	-0.41	0.99	Bootstrap	**0.0002**	832, 1066	8, 11	4, 5
	Low expression *vs* Nasotemporal	Δ locomotion modulation index	0.06	1.22	-0.41	0.99	Bootstrap	**0.0149**	1140, 1066	10, 11	5, 5
	Control *vs* Nasotemporal	Δ locomotion modulation index	0.01	1.02	-0.41	0.99	Bootstrap	**< 10^{-5}**	646, 1066	7, 11	3, 5
	Temporonasal *vs* Nasotemporal	Δ locomotion modulation index	0.05	1.09	-0.41	0.99	Bootstrap	**< 10^{-5}**	1111, 1066	11, 11	5, 5
5C	CT *vs* NR	Locomotion modulation index	-0.14	0.91	0.10	0.87	Bootstrap	**0.0091**	4247, 4383	24,26	19,23
	NT *vs* CT	Locomotion modulation index	0.08	0.92	-0.14	0.91	Bootstrap	**0.0259**	1969, 4247	12, 24	8,19
	NR *vs* NT	Locomotion modulation index	0.10	0.87	0.08	0.92	Bootstrap	0.4309	4383, 1969	26,12	23,8
5E	NR *vs* CT	Locomotion modulation index, fast locomotion	0.07	0.91	-0.24	0.89	Bootstrap	**0.0033**	3042, 2298	16,15	15,12
	NR *vs* CT	Locomotion modulation index, slow locomotion	0.14	0.89	-0.07	0.88	Bootstrap	**0.0152**	4669, 2907	31,18	29,16
	NR *vs* CT	Locomotion modulation index, medium locomotion	0.06	0.93	-0.14	0.89	Bootstrap	**0.027**	4098, 3481	25,21	22,17
5G	Before *vs* After	Locomotion modulation index, fast locomotion	0.29	0.92	-0.24	0.97	Bootstrap	**0.004**	389, 755	4,7	3,4
	Before *vs* After	Locomotion modulation index, medium locomotion	0.34	0.94	-0.03	0.90	Bootstrap	0.0573	872, 723	9,8	5,5
	Before *vs* After	Locomotion modulation index, slow locomotion	0.36	0.91	0.29	0.85	Bootstrap	0.3475	1123, 1043	12,11	5,5
S2B	With *vs* without visual flow	Locomotion onset response (open loop) [% ΔF/F]	3.03	7.82	7.17	6.45	Rank-sum	**0.0442**	n/a	20,14	9,9
S4B	Control *vs* High expression	Pupil diameter response [z-score]	-0.09	0.12	0.14	0.09	Unpaired t-test	**0.0024**	n/a	n/a	7,6
	High expression *vs* Low expression	Pupil diameter response [z-score]	0.14	0.09	0.00	0.05	Unpaired t-test	**0.0071**	n/a	n/a	6,6
	Low expression *vs* Control	Pupil response [z-score]	0.00	0.05	-0.09	0.12	Unpaired T-test	0.1242	n/a	n/a	6,7
S4D	Before *vs* After	Visual response (stationary) [% ΔF/F]	-0.70	3.12	n/a	n/a	Bootstrap	**0.0007**	793	8	4
	Before *vs* After	Visual response (locomotion) [% ΔF/F]	-0.57	3.83	n/a	n/a	Bootstrap	**0.0342**	1163	12	5
	Before *vs* After	Locomotion modulation index	0.01	1.02	n/a	n/a	Bootstrap	0.5637	646	7	3

S4E	Before *vs* After	Locomotion modulation index	0.17	1.01	n/a	n/a	Bootstrap	0.9206	718	7	4
S4F	Before *vs* After	Visual response (stationary) [% ΔF/F]	-0.44	2.31	n/a	n/a	Bootstrap	0.1088	832	8	4
	Before *vs* After	Visual response (locomotion) [% ΔF/F]	-0.07	3.47	n/a	n/a	Bootstrap	0.4273	832	8	4
S6B	NR *vs* CT	Locomotion modulation index, other	0.10	0.94	-0.18	0.87	Bootstrap	**0.0196**	1276, 1384	23,24	22,19
	NR *vs* CT	Locomotion modulation index, NPE	-0.05	0.92	-0.21	0.91	Bootstrap	0.0574	1510, 1108	23,24	22,19
	NR *vs* CT	Locomotion modulation index, PPE	0.10	0.90	-0.06	0.80	Bootstrap	**0.0435**	986, 1755	23,24	22,19
S6D	Before *vs* After	Locomotion modulation index, other	0.34	0.92	-0.14	0.89	Bootstrap	**0.0183**	378, 408	13,13	5,5
	Before *vs* After	Locomotion modulation index, NPE	0.10	0.86	-0.19	0.88	Bootstrap	0.0714	401, 418	13,13	5,5
	Before *vs* After	Locomotion modulation index, PPE	0.50	0.92	0.25	0.81	Bootstrap	0.1094	372, 365	13,13	5,5

REFERENCES

Aston-Jones, G., Bloom, F.E., 1981. Activity of norepinephrine-containing locus coeruleus neurons in behaving rats anticipates fluctuations in the sleep-waking cycle. J. Neurosci. 1, 876–886. https://doi.org/10.1523/JNEUROSCI.01-08-00876.1981

Attinger, A., Wang, B., Keller, G.B., 2017. Visuomotor Coupling Shapes the Functional Development of Mouse Visual Cortex. Cell 169, 1291-1302.e14. https://doi.org/10.1016/j.cell.2017.05.023

Bennett, C., Arroyo, S., Hestrin, S., 2013. Subthreshold mechanisms underlying state-dependent modulation of visual responses. Neuron 80, 350–357. https://doi.org/10.1016/j.neuron.2013.08.007

Bouret, S., Sara, S.J., 2004. Reward expectation, orientation of attention and locus coeruleus-medial frontal cortex interplay during learning. Eur. J. Neurosci. 20, 791–802. https://doi.org/10.1111/j.1460-9568.2004.03526.x

Breton-Provencher, V., Drummond, G.T., Feng, J., Li, Y., Sur, M., 2022. Spatiotemporal dynamics of noradrenaline during learned behaviour. Nature 1–7. https://doi.org/10.1038/s41586-022-04782-2

Chandler, D.J., Jensen, P., McCall, J.G., Pickering, A.E., Schwarz, L.A., Totah, N.K., 2019. Redefining Noradrenergic Neuromodulation of Behavior: Impacts of a Modular Locus Coeruleus Architecture. J. Neurosci. 39, 8239–8249. https://doi.org/10.1523/JNEUROSCI.1164-19.2019

Choi, S.-Y., Chang, J., Jiang, B., Seol, G.-H., Min, S.-S., Han, J.-S., Shin, H.-S., Gallagher, M., Kirkwood, A., 2005. Multiple receptors coupled to phospholipase C gate long-term depression in visual cortex. J. Neurosci. Off. J. Soc. Neurosci. 25, 11433–11443. https://doi.org/10.1523/JNEUROSCI.4084-05.2005

Cox, J., Witten, I.B., 2019. Striatal circuits for reward learning and decision-making. Nat. Rev. Neurosci. 20, 482–494. https://doi.org/10.1038/s41583-019-0189-2

Danskin, B., Denman, D., Valley, M., Ollerenshaw, D., Williams, D., Groblewski, P., Reid, C., Olsen, S., Waters, J., 2015. Optogenetics in Mice Performing a Visual Discrimination Task: Measurement and Suppression of Retinal Activation and the Resulting Behavioral Artifact. PLOS ONE 10, e0144760. https://doi.org/10.1371/journal.pone.0144760

Deitcher, Y., Leibner, Y., Kutzkel, S., Zylbermann, N., London, M., 2019. Nonlinear relationship between multimodal adrenergic responses and local dendritic activity in primary sensory cortices. https://doi.org/10.1101/814657

Dombeck, D.A., Khabbaz, A.N., Collman, F., Adelman, T.L., Tank, D.W., 2007. Imaging Large-Scale Neural Activity with Cellular Resolution in Awake, Mobile Mice. Neuron 56, 43–57. https://doi.org/10.1016/j.neuron.2007.08.003

Dvorkin, R., Shea, S.D., 2022. Precise and Pervasive Phasic Bursting in Locus Coeruleus during Maternal Behavior in Mice. J. Neurosci. Off. J. Soc. Neurosci. 42, 2986–2999. https://doi.org/10.1523/JNEUROSCI.0938-21.2022

Eliades, S.J., Wang, X., 2008. Neural substrates of vocalization feedback monitoring in primate auditory cortex. Nature 453, 1102–1106. https://doi.org/10.1038/nature06910

Erisken, S., Vaiceliunaite, A., Jurjut, O., Fiorini, M., Katzner, S., Busse, L., 2014. Effects of Locomotion Extend throughout the Mouse Early Visual System. Curr. Biol. 24, 2899–2907. https://doi.org/10.1016/j.cub.2014.10.045

Ferguson, K.A., Cardin, J.A., 2020. Mechanisms underlying gain modulation in the cortex. Nat. Rev. Neurosci. 21, 80–92. https://doi.org/10.1038/s41583-019-0253-y

Flagel, S.B., Clark, J.J., Robinson, T.E., Mayo, L., Czuj, A., Willuhn, I., Akers, C.A., Clinton, S.M., Phillips, P.E.M., Akil, H., 2011. A selective role for dopamine in stimulus–reward learning. Nature 469, 53–57. https://doi.org/10.1038/nature09588

Foote, S.L., Aston-Jones, G., Bloom, F.E., 1980. Impulse activity of locus coeruleus neurons in awake rats and monkeys is a function of sensory stimulation and arousal. Proc. Natl. Acad. Sci. U. S. A. 77, 3033–3037.

Greenstreet, F., Vergara, H.M., Pati, S., Schwarz, L., Wisdom, M., Marbach, F., Johansson, Y., Rollik, L., Moskovitz, T., Clopath, C.M., Stephenson-Jones, M., 2022. Action prediction error: a value-free dopaminergic teaching signal that drives stable learning. https://doi.org/10.1101/2022.09.12.507572

He, K., Huertas, M., Hong, S.Z., Tie, X., Hell, J.W., Shouval, H., Kirkwood, A., 2015. Distinct Eligibility Traces for LTP and LTD in Cortical Synapses. Neuron 88, 528–538. https://doi.org/10.1016/j.neuron.2015.09.037

Hervé-Minvielle, A., Sara, S.J., 1995. Rapid habituation of auditory responses of locus coeruleus cells in anaesthetized and awake rats. Neuroreport 6, 1363–1368. https://doi.org/10.1097/00001756-199507100-00001

Jordan, R., Keller, G.B., 2020. Opposing Influence of Top-down and Bottom-up Input on Excitatory Layer 2/3 Neurons in Mouse Primary Visual Cortex. Neuron. https://doi.org/10.1016/j.neuron.2020.09.024

Kasamatsu, T., Pettigrew, J.D., 1976. Depletion of brain catecholamines: failure of ocular dominance shift after monocular occlusion in kittens. Science 194, 206–209. https://doi.org/10.1126/science.959850

Kasamatsu, T., Watabe, K., Heggelund, P., Schöller, E., 1985. Plasticity in cat visual cortex restored by electrical stimulation of the locus coeruleus. Neurosci. Res. 2, 365–386. https://doi.org/10.1016/0168-0102(85)90047-1

Kebschull, J.M., Garcia da Silva, P., Reid, A.P., Peikon, I.D., Albeanu, D.F., Zador, A.M., 2016. High-Throughput Mapping of Single-Neuron Projections by Sequencing of Barcoded RNA. Neuron 91, 975–987. https://doi.org/10.1016/j.neuron.2016.07.036

Keller, G.B., Bonhoeffer, T., Hübener, M., 2012. Sensorimotor mismatch signals in primary visual cortex of the behaving mouse. Neuron 74, 809–815. https://doi.org/10.1016/j.neuron.2012.03.040

Keller, G.B., Mrsic-Flogel, T.D., 2018. Predictive Processing: A Canonical Cortical Computation. Neuron 100, 424–435. https://doi.org/10.1016/j.neuron.2018.10.003

Kim, H.R., Malik, A.N., Mikhael, J.G., Bech, P., Tsutsui-Kimura, I., Sun, F., Zhang, Y., Li, Y., Watabe-Uchida, M., Gershman, S.J., Uchida, N., 2020. A Unified Framework for Dopamine Signals across Timescales. Cell 183, 1600-1616.e25. https://doi.org/10.1016/j.cell.2020.11.013

Leinweber, M., Ward, D.R., Sobczak, J.M., Attinger, A., Keller, G.B., 2017. A Sensorimotor Circuit in Mouse Cortex for Visual Flow Predictions. Neuron 95, 1420-1432.e5. https://doi.org/10.1016/j.neuron.2017.08.036

Liu, Y., Rodenkirch, C., Moskowitz, N., Schriver, B., Wang, Q., 2017. Dynamic Lateralization of Pupil Dilation Evoked by Locus Coeruleus Activation Results from Sympathetic not Parasympathetic Contributions. Cell Rep. 20, 3099–3112. https://doi.org/10.1016/j.celrep.2017.08.094

Martins, A.R.O., Froemke, R.C., 2015. Coordinated forms of noradrenergic plasticity in the locus coeruleus and primary auditory cortex. Nat. Neurosci. 18, 1483–1492. https://doi.org/10.1038/nn.4090

McKinney, A., Hu, M., Hoskins, A., Mohammadyar, A., Naeem, N., Jing, J., Patel, S.S., Sheth, B.R., Jiang, X., 2022. Cellular and Circuit Organization of the Locus Coeruleus of Adult Mice. https://doi.org/10.1101/2022.03.01.481656

Meijering, E., Jacob, M., Sarria, J.-C.F., Steiner, P., Hirling, H., Unser, M., 2004. Design and validation of a tool for neurite tracing and analysis in fluorescence microscopy images. Cytom. Part J. Int. Soc. Anal. Cytol. 58, 167–176. https://doi.org/10.1002/cyto.a.20022

Mu, Y., Bennett, D.V., Rubinov, M., Narayan, S., Yang, C.-T., Tanimoto, M., Mensh, B.D., Looger, L.L., Ahrens, M.B., 2019. Glia Accumulate Evidence that Actions Are Futile and Suppress Unsuccessful Behavior. Cell 178, 27-43.e19. https://doi.org/10.1016/j.cell.2019.05.050

Mukamel, E.A., Nimmerjahn, A., Schnitzer, M.J., 2009. Automated Analysis of Cellular Signals from Large-Scale Calcium Imaging Data. Neuron 63, 747–760. https://doi.org/10.1016/j.neuron.2009.08.009

Niell, C.M., Stryker, M.P., 2010. Modulation of visual responses by behavioral state in mouse visual cortex. Neuron 65, 472–479. https://doi.org/10.1016/j.neuron.2010.01.033

Nomura, S., Bouhadana, M., Morel, C., Faure, P., Cauli, B., Lambolez, B., Hepp, R., 2014. Noradrenalin and dopamine receptors both control cAMP-PKA signaling throughout the cerebral cortex. Front. Cell. Neurosci. 8. https://doi.org/10.3389/fncel.2014.00247

O'Toole, S.M., Oyibo, H.K., Keller, G.B., 2022. Prediction error neurons in mouse cortex are molecularly targetable cell types. https://doi.org/10.1101/2022.07.20.500837

Pakan, J.M., Lowe, S.C., Dylda, E., Keemink, S.W., Currie, S.P., Coutts, C.A., Rochefort, N.L., 2016. Behavioral-state modulation of inhibition is context-dependent and cell type specific in mouse visual cortex. eLife 5, e14985. https://doi.org/10.7554/eLife.14985

Polack, P.-O., Friedman, J., Golshani, P., 2013. Cellular mechanisms of brain-state-dependent gain modulation in visual cortex. Nat. Neurosci. 16, 1331–1339. https://doi.org/10.1038/nn.3464

Rao, R.P., Ballard, D.H., 1999. Predictive coding in the visual cortex: a functional interpretation of some extra-classical receptive-field effects. Nat. Neurosci. 2, 79–87. https://doi.org/10.1038/4580

Reimer, J., McGinley, M.J., Liu, Y., Rodenkirch, C., Wang, Q., McCormick, D.A., Tolias, A.S., 2016. Pupil fluctuations track rapid changes in adrenergic and cholinergic activity in cortex. Nat. Commun. 7, 13289. https://doi.org/10.1038/ncomms13289

Reynolds, J.N.J., Hyland, B.I., Wickens, J.R., 2001. A cellular mechanism of reward-related learning. Nature 413, 67–70. https://doi.org/10.1038/35092560

Roelfsema, P.R., Holtmaat, A., 2018. Control of synaptic plasticity in deep cortical networks. Nat. Rev. Neurosci. 19, 166–180. https://doi.org/10.1038/nrn.2018.6

Sales, A.C., Friston, K.J., Jones, M.W., Pickering, A.E., Moran, R.J., 2019. Locus Coeruleus tracking of prediction errors optimises cognitive flexibility: An Active Inference model. PLOS Comput. Biol. 15, e1006267. https://doi.org/10.1371/journal.pcbi.1006267

Saravanan, V., Berman, G.J., Sober, S.J., 2020. Application of the hierarchical bootstrap to multi-level data in neuroscience. Neurons Behav. Data Anal. Theory 3, https://nbdt.scholasticahq.com/article/13927-application-of-the-hierarchical-bootstrap-to-multi-level-data-in-neuroscience.

Schneider, D.M., Sundararajan, J., Mooney, R., 2018. A cortical filter that learns to suppress the acoustic consequences of movement. Nature 561, 391–395. https://doi.org/10.1038/s41586-018-0520-5

Schultz, W., 2016. Dopamine reward prediction error coding. Dialogues Clin. Neurosci. 18, 23–32.

Schwarz, L.A., Miyamichi, K., Gao, X.J., Beier, K.T., Weissbourd, B., DeLoach, K.E., Ren, J., Ibanes, S., Malenka, R.C., Kremer, E.J., Luo, L., 2015. Viral-genetic tracing of the input–output organization of a central noradrenaline circuit. Nature 524, 88–92. https://doi.org/10.1038/nature14600

Seol, G.H., Ziburkus, J., Huang, S., Song, L., Kim, I.T., Takamiya, K., Huganir, R.L., Lee, H.-K., Kirkwood, A., 2007. Neuromodulators control the polarity of spike-timing-dependent synaptic plasticity. Neuron 55, 919–929. https://doi.org/10.1016/j.neuron.2007.08.013

Shepard, K.N., Liles, L.C., Weinshenker, D., Liu, R.C., 2015. Norepinephrine is necessary for experience-dependent plasticity in the developing mouse auditory cortex. J. Neurosci. Off. J. Soc. Neurosci. 35, 2432–2437. https://doi.org/10.1523/JNEUROSCI.0532-14.2015

Steinberg, E.E., Keiflin, R., Boivin, J.R., Witten, I.B., Deisseroth, K., Janak, P.H., 2013. A causal link between prediction errors, dopamine neurons and learning. Nat. Neurosci. 16, 966–973. https://doi.org/10.1038/nn.3413

Takeuchi, T., Duszkiewicz, A.J., Sonneborn, A., Spooner, P.A., Yamasaki, M., Watanabe, M., Smith, C.C., Fernández, G., Deisseroth, K., Greene, R.W., Morris, R.G.M., 2016. Locus coeruleus and dopaminergic consolidation of everyday memory. Nature 537, 357–362. https://doi.org/10.1038/nature19325

Vankov, A., Hervé-Minvielle, A., Sara, S.J., 1995. Response to novelty and its rapid habituation in locus coeruleus neurons of the freely exploring rat. Eur. J. Neurosci. 7, 1180–1187. https://doi.org/10.1111/j.1460-9568.1995.tb01108.x

Vasilevskaya, A., Widmer, F.C., Keller, G.B., Jordan, R., 2022. Locomotion-induced gain of visual responses cannot explain visuomotor mismatch responses in layer 2/3 of primary visual cortex. https://doi.org/10.1101/2022.02.11.479795

Wagatsuma, A., Okuyama, T., Sun, C., Smith, L.M., Abe, K., Tonegawa, S., 2018. Locus coeruleus input to hippocampal CA3 drives single-trial learning of a novel context. Proc. Natl. Acad. Sci. 115, E310–E316. https://doi.org/10.1073/pnas.1714082115

Widmer, F.C., O'Toole, S.M., Keller, G.B., 2022. NMDA receptors in visual cortex are necessary for normal visuomotor integration and skill learning. eLife 11, e71476. https://doi.org/10.7554/eLife.71476

Yu, A.J., Dayan, P., 2005. Uncertainty, neuromodulation, and attention. Neuron 46, 681–692. https://doi.org/10.1016/j.neuron.2005.04.026

Zmarz, P., Keller, G.B., 2016. Mismatch Receptive Fields in Mouse Visual Cortex. Neuron 92, 766–772. https://doi.org/10.1016/j.neuron.2016.09.057